

***XMM-Newton* EPIC observations of 21 low-redshift PG quasars[★]**

D. Porquet¹, J. N. Reeves^{2,3}, P. O’Brien⁴, and W. Brinkmann¹

¹ Max-Planck-Institut für extraterrestrische Physik, Postfach 1312, 85741, Garching, Germany

² Laboratory for High Energy Astrophysics, NASA Goddard Space Flight Center, Greenbelt, MD 20771, USA

³ Universities Space Research Association

⁴ Department of Physics and Astronomy, University of Leicester, Leicester LE1 7RH, UK

Received 20 January 2004 / Accepted 8 April 2004

Abstract. We present an X-ray spectral analysis of 21 low redshift quasars observed with *XMM-Newton* EPIC. All the sources are Palomar Green quasars with redshifts between 0.05 and 0.4 and have low Galactic absorption along the line-of-sight. A large majority of quasars in the sample (19/21) exhibit a significant soft excess below ~ 1 –1.5 keV, whilst two objects (PG 1114+445 and IZw1) show a deficit of soft X-ray flux due to the presence of a strong warm absorber. Indeed, contrary to previous studies with *ASCA* and *ROSAT*, we find that the presence of absorption features near 0.6–1.0 keV is common in our sample. At least half of the objects appear to harbor a warm absorber, as found previously in Seyfert 1 galaxies. We find significant detections of Fe $K\alpha$ emission lines in at least twelve objects, whilst there is evidence for some broadening of the line profile, compared to the EPIC-pn resolution, in five of these quasars. The determination of the nature of this broadening (e.g., Keplerian motion, a blend of lines, relativistic effects) is not possible with the present data and requires either higher *S/N* or higher resolution spectra. In seven objects the line is located between 6.7–7 keV, corresponding to highly ionized iron, whereas in the other five objects the line energy is consistent with 6.4 keV, i.e. corresponding to near neutral iron. The ionized lines tend to be found in the quasars with the steepest X-ray spectra. We also find a correlation between the continuum power law index Γ and the optical $H\beta$ width, in both the soft and hard X-ray bands, whereby the steepest X-ray spectra are found in objects with narrow $H\beta$ widths, which confirms previous *ROSAT* and *ASCA* results. The soft and hard band X-ray photon indices are also strongly correlated, i.e. the steepest soft X-ray spectra correspond the steepest hard X-ray spectra. We propose that a high accretion rate and a smaller black hole mass is likely to be the physical driver responsible for these trends, with the steep spectrum objects likely to have smaller black hole masses accreting near the Eddington rate.

Key words. galaxies: quasars: general – X-rays: general – galaxies: nuclei – radiation mechanisms : general

1. Introduction

In Active Galactic Nuclei (AGN), from Seyfert galaxies to quasars, the analysis of spectral X-ray features can help us to understand the central regions of these powerful objects. The first is the so-called soft excess seen below 2–3 keV (Arnaud et al. 1985; Turner & Pounds 1989). This spectral characteristic is thought to be the high energy part of the optical-UV “big blue bump” extending down to 1 μm , which contains a large fraction of the bolometric luminosity. Soft X-ray excesses were detected for most AGN with *ROSAT* (e.g., Brinkmann 1992; Buehler et al. 1995). Using *XMM-Newton* observations, Pounds & Reeves (2002), recently confirmed the presence of a soft X-ray excess in all objects of their sample (6 Seyfert galaxies), with amplitude and width increasing with luminosity. Current

interpretations of the soft excess range from direct thermal emission from the accretion disk to reprocessing of harder radiation absorbed in the thin disk (Pounds & Reeves 2002). Other important components are emission and/or absorption structures, mainly in the soft X-ray range, due to a warm absorbing medium supposed to be located between the Broad Line Region and the Narrow Line Region (e.g., Reynolds & Fabian 1995; Porquet et al. 1999). These absorption and/or emission features are commonly seen in low-luminosity AGN such as Seyfert galaxies, but are rather rare in quasars. The Fe $K\alpha$ line complex observed in the 6–7 keV range is also an important spectral diagnostic tool to probe dense matter from the inner disk (e.g., MCG-06-30-15, Tanaka et al. 1995; Fabian et al. 2002; Q0056-363, Porquet & Reeves 2003) to the Broad Line Region and the molecular torus (e.g. NGC 5548, Yaqoob 2001; Mrk 205, Reeves et al. 2001; Mrk 509, Pounds et al. 2001). Recently, Page et al. (2004) have shown that the majority of 53 AGN observed with *XMM-Newton*, including both Seyfert 1 and quasars, exhibit narrow Fe K line near 6.4 keV, due to the

Send offprint requests to: D. Porquet,

e-mail: dporquet@mpe.mpg.de

[★] Appendix A and Tables 2–12 are only available in electronic form at <http://edpsciences.org>

Table 1. The 21 Type I AGN included in the present sample. The Galactic column density along the line-of-sight ($N_{\text{H}}^{\text{Gal}}$) is expressed in units of 10^{20} cm^{-2} . NLG: narrow line galaxy. RQQ: radio-quiet quasar. RLQ: radio-loud quasar.

Source	Other name	Coordinates (J2000)		z	$N_{\text{H}}^{\text{Gal}}$	M_{v}	R_{L}	$FWHM(\text{H}\beta)$ km s $^{-1}$	Type
		RA	Dec						
PG 0050+124	IZw1	00 53 35.08	+12 41 34.4	0.061	4.94	-23.77	-0.48	1240	NLG
PG 0804+761		08 10 58.66	+76 02 42.5	0.100	3.01	-24.44	-0.22	3070	RQQ
PG 0947+396	K347-45	09 50 48.39	+39 26 50.6	0.206	1.55	-24.21	-0.60	4830	RQQ
PG 0953+414	K348-7	09 56 52.41	+41 15 22.1	0.239	0.82	-25.65	-0.36	3130	RQQ
PG 1048+342		10 51 43.88	+33 59 26.9	0.167	1.94	-24.02	-1.00	3600	RQQ
PG 1114+445		11 17 06.40	+44 13 33.2	0.144	1.62	-24.01	-0.89	4570	RQQ
PG 1115+407		11 18 30.30	+40 25 53.8	0.154	1.91	-23.74	-0.77	1720	NLG
PG 1116+215	TON 1388	11 19 08.60	+21 19 18.0	0.177	1.29	-25.57	-0.14	2920	RQQ
PG 1202+281	GC Com	12 04 42.11	+27 54 11.5	0.165	1.70	-23.75	-0.72	5050	RQQ
PG 1244+026		12 46 35.29	+02 22 08.3	0.048	1.78	-21.77	-0.28	830	NLG
PG 1307+085		13 09 47.03	+08 19 49.3	0.155	2.10	-24.56	-1.00	2360	RQQ
PG 1309+355	TON 1565	13 12 17.74	+35 15 21.3	0.184	1.02	-24.76	+1.26	2940	RLQ
PG 1322+659		13 23 49.54	+65 41 48.0	0.168	2.00	-24.23	-0.92	2790	RQQ
PG 1352+183	PB 4142	13 54 35.93	+18 05 18.1	0.152	2.05	-24.13	-0.96	3600	RQQ
PG 1402+261	TON 182	14 05 16.21	+25 55 34.1	0.164	1.47	-24.48	-0.64	1910	NLG
PG 1426+015	Mrk 1383	14 29 06.59	+01 17 06.5	0.086	2.85	-24.05	-0.55	6820	RQQ
PG 1427+480		14 29 43.08	+47 47 26.3	0.221	1.86	-24.04	-0.80	2540	RQQ
PG 1440+356	Mrk 478	14 42 07.46	+35 26 22.9	0.077	1.04	-23.49	-0.43	1450	NLG
PG 1512+370	4C 37.43	15 14 43.06	+36 50 50.5	0.371	1.35	-25.93	+2.28	6810	RLQ
PG 1613+658	Mrk 876	16 13 57.18	+65 43 09.6	0.129	2.85	-24.22	+0.00	8450	RQQ
PG 1626+554		16 27 56.09	+55 22 31.7	0.132	2.02	-23.54	-0.96	4490	RQQ

emission from neutral material, such as the BLR or the putative molecular torus.

In this paper, we present the spectral analysis of a sample of 21 low-redshift quasars ($z \sim 0.05\text{--}0.4$), obtained with *XMM-Newton*. One great advantage of such study with the EPIC cameras (MOS and pn) is the combination of high sensitivity with moderate spectral resolution over a broad energy band, i.e. from 0.3 keV up to 12 keV for the pn camera. All sources are Palomar Green objects (Green et al. 1986) with low absorption column density along the line-of-sight. Note that all fit parameters given in this paper are in the quasars rest frame, with values of $H_0 = 75 \text{ km s}^{-1} \text{ Mpc}^{-1}$, and $q_0 = 0.5$ assumed throughout.

In Sect. 2, we present the quasar sample used in this work as well as the data reduction techniques. In Sect. 3, we estimate the accretion rate with respect to the Eddington rate for each quasar. In Sect. 4, we analyze the spectral shapes over different energy bands. The possible presence of a warm absorber medium and of a Fe K line is checked in Sects. 5 and 6, respectively. Then, in Sect. 7, we investigate possible potential origins for the soft excess and which model could account for the whole spectral shape. Finally, in Sect. 8, we report the global properties of the quasar sample and check for correlations between the X-ray properties and other quasar properties. In Appendix A, we report individual notes about each object of our sample.

2. *XMM-Newton* observations

2.1. The sample

We present archival *XMM-Newton* observations of 21 low-redshift quasars. In Table 1, we report for each object: coordinates; redshift from Schmidt & Green (1983); Galactic column density along the line-of-sight ($N_{\text{H}}^{\text{Gal}}$); visual absolute magnitude (M_{v}) from Boroson & Green (1992); ratio of radio to optical luminosity (radio-loudness R_{L} , in logarithmic scale) as defined in Kellerman et al. (1989); Full Width at Half Maximum ($FWHM$) of the $\text{H}\beta$ line at 5100 Å from Boroson & Green (1992), and the object type. The Galactic column density values have been obtained from the COLDENs program using the compilations of Dickey & Lockman (1990). Five objects can be classified as narrow line galaxies (NLG) with $FWHM \leq 2000 \text{ km s}^{-1}$: IZw1, PG 1115+407, PG 1244+026, PG 1402+261, and Mrk 478; and two are radio-loud quasars (RLQ) with $R \geq 1.0$: PG 1309+355, and PG 1512+370. The other 14 objects are radio-quiet quasars (RQQ). The Palomar Bright Quasar Survey (BQS) contains 114 objects (see Kellerman et al. 1989), including 72 quasars with redshift between 0.048 and 0.400. Taking the values of M_{v} and $FWHM(\text{H}\beta)$ from Boroson & Green (1992), we found for these 72 objects that the values span a large range: $-21.43 \leq M_{\text{v}} \leq -27.15$ and $830 \leq FWHM(\text{H}\beta) \leq 9410 \text{ km s}^{-1}$. The corresponding average values are -24.3 ($\sigma = 1.2$) and 3712 km s^{-1}

($\sigma = 1980 \text{ km s}^{-1}$) respectively. The present 21 objects represent about one third of the latter objects, and the values of Mv and $FWHM(H\beta)$ also cover a large range: $-21.77 \leq Mv \leq -25.93$ and $830 \leq FWHM(H\beta) \leq 8450 \text{ km s}^{-1}$. The corresponding average values are -24.2 ($\sigma = 0.9$) and 3577 km s^{-1} ($\sigma = 1933 \text{ km s}^{-1}$), respectively. Therefore the present subsample can properly represent the properties of the larger sample of low-redshift PG quasars, without any obvious bias towards Mv and $FWHM(H\beta)$.

2.2. Data reduction and analysis

Table 2 reports for each object in the sample: the observation date, the corresponding *XMM-Newton* orbit revolution, the observation ID, and the exposure time. The EPIC MOS cameras (Turner et al. 2001) were operated in large window mode, except for IZw1 and PG 1307+085 (small window mode), and for PG 1244+026 and Mrk 1383 (full window mode). The EPIC pn camera (Strüder et al. 2001) was also operated in Large Window mode, except for PG 0804+761, PG 1244+026, Mrk 1383, and Mrk 876 (full window mode). For all observations the thin filter was used, except for IZw1 (medium filter). The data were re-processed and cleaned using the *XMM-Newton* SAS VERSION 5.4.1 (Science Analysis Software) package. Since pile-up effects are negligible, X-ray events corresponding to patterns 0–12 and 0–4 (singles and doubles) are selected from the MOS and pn cameras, respectively; except in the case of Mrk 1383 for which we use only single events. As reported recently by Kirsch (2003), significant differences occurred in the low energy redistribution characteristics of the MOS cameras compared to early observations. This means that from approximately revolution 450 onwards the calibration below 500 eV is suspect for the MOS. Therefore for observations with a revolution number above 440, we use a low energy cutoff at 500 eV for the MOS data, and a cutoff at 300 eV for the other MOS data and for all pn data. Since the pn CCD has higher sensitivity and a broader energy range (0.3–12 keV), we use the time-averaged pn spectrum for each object for the spectral analysis (except for PG 0804+761 for which only MOS data are usable). Indeed pn spectra are better suited for the detection of Fe K line and the analysis of the soft excess down to 0.3 keV. However, we have checked that the results obtained from the pn data are consistent with those from the MOS data. The spectra are binned to give a minimum of 100 counts per bin for IZw1, and of 40 counts per bin for PG 0953+414, PG 1048+342, PG 1114+445, PG 1202+281. The other spectra are binned to give a minimum of 20 counts per bin.

The errors quoted correspond to 90% confidence ranges for one interesting parameter ($\Delta\chi^2 = 2.71$). Abundances are those of Anders & Grevesse (1989). In the following, we use the updated cross-sections for X-ray absorption by the interstellar medium from Wilms et al. (2000).

F-Tests are performed (Bevington & Robinson 1992) to estimate the significance of spectral features such as emission lines and absorption edges. Only features detected with a significance greater than 90% are considered.

3. Quasar accretion rate with respect to the Eddington rate

In this section, the accretion rates are estimated with respect to the Eddington rate, defined as:

$$\dot{m} = \frac{\dot{M}}{\dot{M}_{\text{Edd}}} = \frac{L_{\text{bol}}}{L_{\text{Edd}}} = \frac{L_{\text{bol}}}{1.26 \times 10^{38} M_{\text{BH}}}, \quad (1)$$

where \dot{M} and \dot{M}_{Edd} are the quasar mass accretion rate and the Eddington accretion rate (in $M_{\odot} \text{ yr}^{-1}$), respectively; L_{bol} and L_{Edd} are the bolometric and Eddington luminosities (in erg s^{-1}), respectively; and M_{BH} is the black hole mass (in M_{\odot}). In Table 3, the following values are reported: Col. (1) the black hole mass (expressed in M_{\odot}); Col. (2) the monochromatic luminosity $\nu L_{\nu}(5100 \text{ \AA})$ (in erg s^{-1}); Col. (3) the bolometric luminosity (in erg s^{-1}), and Col. (4) the accretion rate with respect to Eddington rate (\dot{m}). The bolometric luminosities (in erg s^{-1}) are from Woo & Urry (2002), Grupe et al. (2004), or are estimated by using the approximation: $L_{\text{bol}} \approx 9 \times \nu L_{\nu}(5100 \text{ \AA})$ reported in Kaspi et al. (2000). Woo & Urry (2002) calculated the bolometric luminosities either from spectral energy distribution (SED) fitting or by flux integration. Grupe et al. (2004) estimated the bolometric luminosities by a combined power law with exponential cut-off to the optical-UV data and an absorbed power law to the soft X-ray data. The accretion rates reported here are only approximations since both the estimates of the bolometric luminosities and of the black hole masses are subject to uncertainties. The determination of the bolometric luminosity is affected by spectral variability and lack of wavelength coverage, mainly in the UV band near 912 \AA , where most of the luminosity is emitted, due to absorption by Galactic neutral hydrogen. As shown by Ferrarese et al. (2001), the black hole masses inferred, from reverberation mapping (mean, rms) and from M_{BH} versus stellar velocity relation, are consistent with each other.

4. *XMM-Newton* spectra

In all subsequent fits (except when considering an absorbed power law fit to the 2–5 keV range where we only use Galactic absorption), the column density is fitted with two components: a Galactic column fixed to the values reported in Table 1 ($N_{\text{H}}^{\text{Gal}}$), as well as possible intrinsic absorption (N_{H}^{in}) in the QSO rest frame, which is allowed to vary.

A single absorbed power law model over the total 0.3–12 keV energy range gives a poor fit for all sources in the sample. To characterize the hard X-ray continuum, we fit an absorbed power law model over the 2–5 keV energy range where the spectra should be relatively unaffected by the presence of a broad soft excess, of a warm absorber-emitter medium, of a Fe K_{α} emission line, and of a contribution from a high energy Compton reflection hump above 8 keV. In this energy range, all spectra are well fitted by a single power law model (Table 4). The X-ray emission of the sample in this energy band covers a wide range of photon indices from hard (e.g., $\Gamma \sim 1.4$ for PG 1114+445 and PG 1307+085) to soft (e.g., $\Gamma \sim 2.5$ for PG 1244+026). Figure 1 displays the data/model ratio fit in the 2–5 keV energy range, extrapolated over the 0.3–12 keV energy

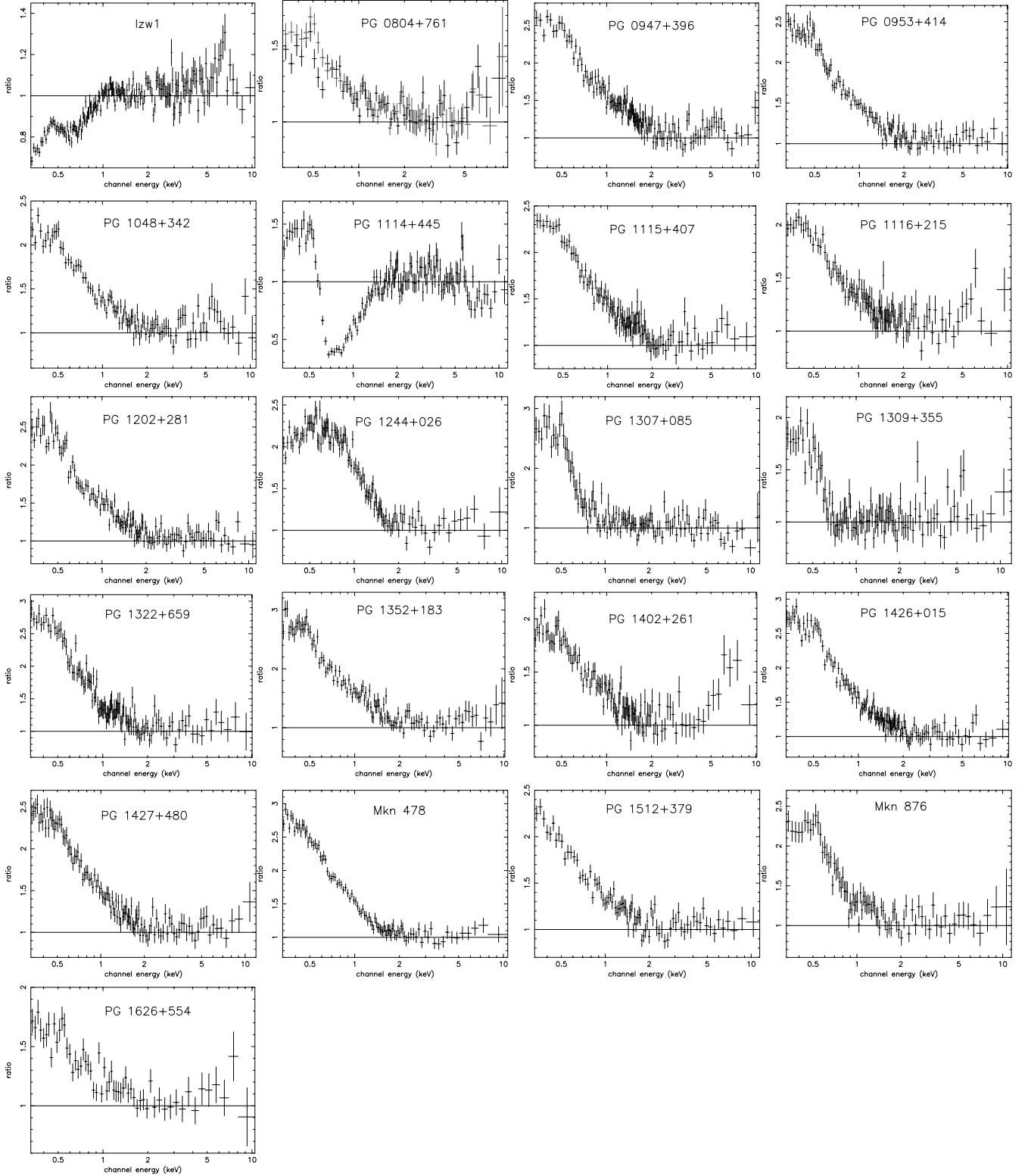


Fig. 1. Data/model ratio of an absorbed power law fit to the 2–5 keV energy range extrapolated over the 0.3–12 keV energy range for the 21 objects of the sample (observer frame).

band. All objects exhibit a positive excess below 1–1.5 keV, the so-called soft excess, except IZw1, and PG 1114+445, which display very significant negative deviations in the soft part of the spectrum. PG 1114+445 exhibits a huge absorption feature between 0.6 and 1.5 keV.

Fitting the soft part (0.3–2 keV) with an absorbed power law model, we obtain a good fit for 12 objects (see Table 4). The inferred photon indices ($2.0 \leq \Gamma \leq 3.1$) correspond to steep spectra. We show below that for some objects the addition

of one or two absorption edges improves the fit in this energy band significantly.

Next we fit the data with a broken power law model to take into account the soft and hard spectral shapes. As reported in Table 5, all objects are well described by this continuum model, except for the two Narrow Line type objects IZw1 and PG 1244+026, and for the RQQ PG 1114+445. For IZw1 and PG 1114+445 this is due to the presence of a strong absorption feature(s) below 1 keV. For PG 1244+026, the soft X-ray shape appears more curved than for the other objects (Fig. 1).

5. The warm absorber

The first detection of the signature of a warm absorber (WA) located inside an AGN was the absorption edges of O VII (0.74 keV) and O VIII (0.97 keV) in the quasar MR 2251-158 (Halpern 1984) with the *Einstein* observatory. Such features were commonly observed in Seyfert 1 galaxies with *ASCA* (e.g., Reynolds & Fabian 1995; Reynolds 1997; George et al. 1998). However, this highly ionized medium is not only an absorber but also an emitter as predicted by Netzer (1996), and confirmed by the new generation of X-ray satellites *Chandra* and *XMM-Newton* which have revealed the very complex soft X-ray spectra of Seyfert galaxies (e.g., Kaspi et al. 2001; Kaastra et al. 2002; Kinkhabwala et al. 2002). For Seyfert 1 galaxies, numerous absorption features (and a few emission features) have been found, while for Seyfert 2 galaxies only emission features were detected. This is in good agreement with the Unified Scheme, where in the case of Seyfert 2 galaxies the central X-ray source is hidden by a molecular torus, thus the WA is only detected in emission. However in quasars, the detection of a WA appeared to be very rare (e.g., Reeves & Turner 2000; George et al. 2000), and only a few detections have been reported with *ASCA* and *ROSAT*; for example at low redshifts MR 2251-158 ($z = 0.06$) by Halpern (1984); and at higher redshifts PG 1114+445 ($z = 0.144$) by Reeves & Turner (2000), and PDS 456 ($z = 0.184$) by Reeves et al. (2003). Recently with *XMM-Newton*, Brinkmann et al. (2004a) reported absorption and emission features in the soft X-ray part of two X-ray weak quasars PG 1411+442 and Mrk 304, strongly suggesting the presence of ionized material in the central region of these two sources.

In our sample, IZw1 clearly shows absorption features below 1 keV, while PG 1114+445 has a huge absorption trough between 0.6 and 1.5 keV as displayed in Fig. 1. We now describe the spectral analysis of these features for these two objects, and we also check for such signatures of the WA in the other quasars. We first fit the spectra combining an absorbed broken power law with two absorption edges of O VII and O VIII. For PG 1114+445, a single underlying power law model is used. The energies of the edges are initially fixed to their rest frame values at 0.74 keV and 0.87 keV respectively (see results in Table 6). There are six significant detections above about 99% confidence. Then, in order to allow for a possible outflow or inflow of the WA, we leave the energies of the absorption edges as free parameters. We find significant detections (>99% compared to the continuum alone) of absorption edges in ten objects: IZw1, PG 0804+761, PG 0947+396,

PG 1114+445, PG 1115+407, PG 1202+281, PG 1307+085, PG 1309+355, PG 1352+183, and Mrk 876. We do not claim that the absorption features found here are from oxygen edges but due to the low resolution of EPIC data below 1 keV, we fit the data with one or two absorption edges as a simple parameterisation only. Indeed the detected absorption features could also correspond to absorption lines from N, O or Ne as well as Unresolved Transition Arrays (UTA, Behar et al. 2001) of absorption from low ionization (Fe < XVII) iron L-shell lines as recently found in IRAS 13349+2438 with *XMM-Newton*/RGS (Sako et al. 2001). In addition, the presence of narrow absorption lines in some objects cannot be inferred with the lower resolution EPIC data presented here. Therefore, the determination of the exact nature (ionization parameter, outflow velocity, etc.) of the WA and of its complexity, as well as the exact fraction of objects exhibiting a warm absorber, require a much more detailed analysis with the higher spectral resolution of the RGS, which will be presented in a forthcoming paper. In conclusion, here we found that at least half of the 21 objects probably show evidence for absorption features.

6. The Fe K_{α} line

Next we check for the presence of a Fe K_{α} line in each spectrum. Indeed as shown in Fig. 1 some spectra exhibit a positive deviation at about 6.4–7 keV compared to the continuum. Figure 2 displays a zoom of these features (data/continuum ratio) for six objects (IZw1, PG 0804+761, PG 1114+445, PG 1116+215, PG 1309+355, and PG 1402+261). We add a Gaussian line to the absorbed broken power law model in the 0.3–12 keV energy range (including absorption edges when required), except in the case of PG 1244+026 where we fit a simple power law continuum in the 2–12 keV energy range. Table 7 reports the parameters of the fitted lines. $F_{\text{prob}}^{\text{line}}$ is the “significance” of the line compared to the continuum model alone (only detections with $F_{\text{prob}}^{\text{line}} \geq 90\%$ are quoted). First we fix the width of the line at 10 eV, i.e. the line is intrinsically narrow, much narrower than the resolution of the EPIC-pn at this energy. We find evidence of a Fe K shell emission line in at least twelve objects. In five objects the line energy is consistent within the errors to “neutral” or moderately ionized iron near 6.4 keV (i.e. $\leq \text{Fe XVII}$): PG 0947+396, PG 1048+342, PG 1114+445, PG 1309+355, and PG 1512+379. For the other seven objects the line energy is consistent with highly ionized iron: IZw1, PG 0804+761, PG 1115+407, PG 1116+215, PG 1244+026, PG 1402+261, and Mrk 1383. We notice that for PG 0947+396, PG 1115+407, PG 1244+026, PG 1309+355, Mrk 1383, and PG 1512+379 the detections are less significant, between 90–99% confidence.

For five objects the fit is statistically improved ($F_{\text{prob}}^{\text{broad}} \geq 90\%$) allowing the width of the line to vary as a free parameter. In three objects the detection of a broad line is highly significant at >99% confidence: IZw1, PG 1116+215 and PG 1402+261. The inferred *FWHM* are very large with $64\,000_{-32\,000}^{+56\,000}$ km s⁻¹, $76\,000_{-33\,000}^{+51\,000}$ km s⁻¹, and $115\,000_{-39\,000}^{+61\,000}$ km s⁻¹, respectively. In two objects (PG 0804+761 and PG 1309+355) allowing the line to be broad results in a less significant (90–99%) improvement of the fit

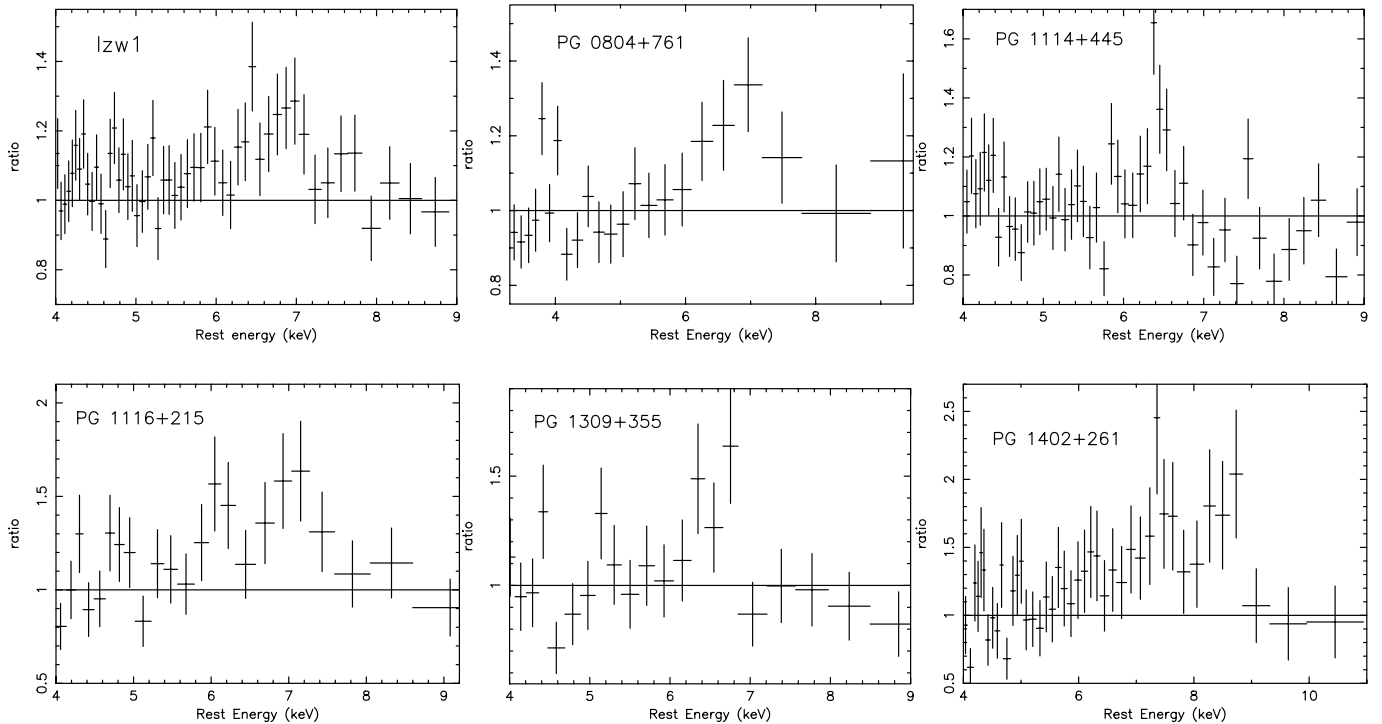


Fig. 2. Details of the iron line profiles (data/model ratio as in Fig. 1, in observer frame) for the six objects which show lines at very high confidence level.

statistic. We find smaller $FWHM$ $59\,000^{+58\,000}_{-23\,000}$ km s^{-1} , and $23\,000^{+26\,000}_{-11\,000}$ km s^{-1} , respectively. For PG 1309+355, the S/N is not sufficient to distinguish between a real broad line and a possible blend of a 6.4 keV line with another ionized iron line. For three objects exhibiting both a broad and a highly ionized iron line (IZw1, PG 0804+761, PG 1116+215), the broadening could be due to blend of several ionized iron lines. For example, according to the detailed analysis of the data of IZw1, Gallo et al. (2004) proposed that the broad iron emission feature can be attributed to a neutral line and a blend of He- and H-like lines. However for PG 1402+261, the line appears to be blueshifted to 7.3 keV (from the broad Gaussian fit) beyond the laboratory energy of H-like iron K_{α} fluorescent transition, and it is therefore unlikely to result from a blend of ionized lines between 6.4 keV and 7.0 keV.

For the five objects showing a broad Fe K line, we check for possible relativistic effects. Therefore, we fit a relativistic line profile: DISKLINE from Fabian et al. (1989), and LAOR from Laor (1991) for a non-rotating Schwarzschild BH and a rapidly rotating Kerr BH, respectively. These relativistic line profiles give a good fit for all objects. For PG 1402+261, the rest-energy of the line is very high ($E \sim 8.5$ – 8.6 keV) when fitted with an AD inclination (θ) fixed at 30 degrees. This either implies that the disk is highly inclined to the line-of-sight ($\theta = 69^{+8}_{-4}$ deg, $E = 6.9^{+0.3}_{-0.6}$ keV), or that the matter is outflowing with a velocity of about 0.2 – $0.3c$ assuming a very highly ionized line at 6.7–7 keV. The complex Fe K line profile of PG 1402+261 will be investigated in much more detail in a subsequent paper (Reeves et al. 2004). No significant difference has been found comparing the χ^2 obtained for the relativistic

line profile and for a broad Gaussian line. The width of the Gaussian lines could be due to a blend of several ionized lines or simply due to Keplerian motion. With the present S/N data we are not able to infer the incidence of real relativistic effects in these quasars. Higher S/N data or better spectral resolution are needed for such an investigation.

For the five objects showing a significant Fe K line consistent with 6.4 keV (PG 0947+761, PG 1048+342, PG 1114+445, PG 1309+355, PG 1512+370), neither a broad line (as reported in Table 7), nor an additional broad component (i.e. in addition to the narrow line), are significantly required (i.e., at a confidence level greater than 90%). As shown previously by Porquet & Reeves (2003), broad and intense neutral iron lines in quasars appear to be very rare, with the quasar Q0056-363 being the most luminous quasar found to date showing such characteristics. Interestingly, four of the five NLG in the sample show evidence for a highly ionized Fe K line: IZw1, PG 1115+407, PG 1244+026, and PG 1402+261. Five RQQ in our sample show the significant presence of a Fe K line, from which only two correspond to highly ionized iron: PG 0804+761 and PG 1116+215. These latter two objects have relatively steep 2–5 keV photon indices of about 2.2–2.3. Objects with line energies at about 6.4 keV seem to be related to flatter spectra with $\Gamma \sim 1.4$ – 1.9 . The RLQ PG 1309+355 displays the presence of a “neutral” Fe K line, whilst the detection of such a line in PG 1512+379 is less significant. Both objects are characterized by a flat photon index of about 1.7. These results are consistent with the correlations found between the Fe K line energy and the 2–10 keV X-ray power law slope by Dewangan (2002). This indicates that steep X-ray spectrum

objects (such as NLG) tend to have highly ionized (e.g. He or H-like) Fe K line emission, while flatter hard X-ray spectra tend to be associated with neutral or weakly ionized material. We check this by testing for Spearman-rank correlations between the line energy versus the 2–5 keV photon index. We find a significant positive correlation between both parameters with a probability of 99.7%. This correlation between line energy and photon index is consistent with ionized disk reflection models; in this scenario the disk iron line emission tends to be highly ionized (e.g. He or H-like iron) when the photoionizing continuum is steep, and stronger than the emission from neutral iron (e.g. Nayakshin et al. 2000; Ross et al. 1999). This is due to the formation of a highly ionized layer of iron near the accretion disk skin. Therefore one expects to see strong ionized iron emission lines in NLGs.

6.1. X-ray disk reflection model

Given the evidence for broad iron lines in five objects, where the emission is likely to originate from the inner accretion disk (AD), we attempt to fit the X-ray spectra of these objects with a disk reflection model in the 2–12 keV energy range. We use the ionized disk reflection model XION of Nayakshin et al. (2000), in the most simple configuration where the X-rays are emitted in a “lamppost” geometry at a height h above the AD. For this LAMPOST model, we assume a height h for the X-ray source above the disc of $10 R_g$, a ratio of X-ray to disk flux of 0.2, an outer AD radius of $1000 R_g$, a solar iron abundance, and a high energy cut-off of 100 keV for the emitting source. The accretion rate is fixed to the value reported in Table 3. The AD inclination (in deg), and the inner AD radius are free parameters. For PG 1402+261, we need to vary some of the reflection parameters to achieve a good fit. We find a lower height for the X-ray source above the AD of about $2.5 R_g$, required to make the emission more centrally concentrated around the black hole, whilst an iron overabundance of 5 relative to solar is required (the maximum the XION model allows) in order to fit the extreme strength ($EW \sim 2$ keV) of the line. Even with this high abundance for PG 1402+261, we find that the spectrum is dominated by the reflected emission from the disc, with the hard X-ray power law not directly observed (Reeves et al. 2004). For the other objects, the spectrum is not dominated by the reflection component which contributes less than about 10% of the total flux at 6 keV. All fit results are reported in Table 8. For all five objects, this ionized disk reflection model gives a good representation of the data over the 2–12 keV energy range both for the underlying continuum and the Fe K_α line.

In order to check whether the soft excess can also be explained by this model, we extrapolate the above fits over the broad 0.3–12 keV energy range. Even when leaving the parameters free to vary and adding one or two absorption edges if required, we find a bad representation of the overall spectral shape for the four objects with a large soft excess. Therefore, the soft excess in these objects cannot be solely due to reprocessing of the primary X-ray component by an ionized disk, as found also for Mrk 896 (Page et al. 2003a) and for Q 0056-363 (Porquet & Reeves 2003). For IZw1, PG 0804+761 and

PG 1114+445 which show a weak or no soft excess, the overall spectra are well fitted by an ionized disk reflection model.

7. The broad band spectra: Soft X-ray excess and hard tail

7.1. Thermal emission from the accretion disk?

The standard explanation for the soft X-ray excess is that it results from thermal emission originating directly from the hot inner AD (Malkan & Sargent 1982), and hence it is the high energy tail of the so-called Big Blue Bump. We fit the data with the combination of an AD black body spectrum (DISKPN in XSPEC, Gierliński et al. 1999) and a power law model, for the soft and hard band, respectively. The results are reported in Table 9. The maximal values of the disk temperature calculated for a standard α thin accretion disk at $3 R_S$ (Peterson 1997) are reported in the second column of Table 9 ($T_{\text{disk}}^{\text{max}}$ in eV), using the values of M_{BH} and \dot{m} given in Table 3. The spectra of all objects are well represented by this model. For PG 1114+445 no disk black body emission is required due to the deep warm absorber present in this object. We see that the inferred black body temperatures obtained for the objects appear to be too hot to originate directly from emission of a standard α thin accretion disk. The only possible exception may be PG 1244+026 which has the highest black body to power law flux ratio below 2 keV. This quasar has the lowest black hole mass and highest Eddington accretion rate in the sample, thus one may expect a hotter AD for this object.

7.2. Compton scattering?

As an alternative to the thermal emission model for the soft X-ray excess, reprocessing in the form of Compton up-scattering may explain the soft X-ray shape. For example the accretion disk may be responsible for the EUV emission, with some of these soft photons being inverse-Compton scattered into the X-ray energy range, as they pass through the hot corona above the disk. Therefore we investigate such models over the 0.3–12 keV range, by using the COMPTT model in XSPEC (Titarchuk 1994), using a disk geometry. We first test a model with one absorbed COMPTT component, however we obtain unsatisfactory fits as this model failed to account the soft X-ray curvature observed in most of the spectra. Then we assume that there are two Comptonising regions with different temperatures and optical depths. We fix the input soft photons temperature (kT_{photon}) of the cooler COMPTT component to the corresponding value of $T_{\text{disk}}^{\text{max}}$ reported in Table 9 (second column), which is representative of the inner accretion disk temperature. Since our spectral bandpass (up to 12 keV) does not enable us to constrain the temperature of the hotter COMPTT component, we use a power law model which is a good representation for a hotter component with a kT_{plasma} of typically 100 keV (Titarchuk & Lyubarskij 1995). The inferred parameters are reported in Table 10. The data are typically fitted with kT_{plasma} between 0.1 and 0.4 keV for the cooler region, except for PG 0804+761 and PG 1114+445 which exhibit much higher temperature of about 3 keV. However the parameters (kT_{plasma} and τ) are

subject to the inherent degeneracy of the Comptonization models, due to the limited bandpass, as pointed out by Brinkmann et al. (2004b).

In most of the objects in the present sample, the soft X-ray excess is too hot to result directly from the inner accretion disk. Thus a more realistic physical explanation requires Comptonization of soft (EUV) disk photons in a hot plasma. The electron temperature of this soft component is typically a few hundred eV, whilst the optical depth is high ($\tau \gg 1$), the result being that the soft X-ray excess resembles a broadened or smeared black body component, with an output temperature similar to the electron temperature. This readily explains the shape of the soft X-ray excess observed in many other AGN to date with *XMM-Newton*, which can often be fit with multiple black body components (e.g. PKS 0558-504, O'Brien et al. 2001; 1H 0419-577, Page et al. 2002). The power law like component observed above 2 keV is then likely to arise from a second much hotter (or even non-thermal) Comptonizing component, where the high energy roll-over is expected to be situated outside the *XMM-Newton* bandpass.

A plausible physical scenario is that the hard X-ray emission from the hot Comptonizing component heats the surface of the disk which then emits the cooler soft X-ray component that is responsible for the soft excess. One problem with this model is the compactness of the soft X-ray emission component. The soft Comptonized emission can be approximated by a black body as it is optically thick. Thus taking typical values from the sample for the soft excess temperature ($T \sim 10^6$ K), soft luminosity (10^{44} erg s $^{-1}$) and black hole mass ($10^8 M_\odot$), the size of the soft X-ray emitting region would only be $R \sim 10^{12}$ cm or 0.1 gravitational radii (R_g). Thus the soft X-ray component has to be very compact, even for the scenario where it is heated by intense hard X-ray flares above the disk surface.

7.3. A relativistically smeared partially ionized absorber?

Recently, Gierliński & Done (2004) suggested an alternative origin for the soft excess for radio-quiet quasars. They proposed that “the soft X-ray excess is an artefact of strong, relativistically smeared, partially ionized absorption”. Such absorption requires very steep ($\Gamma \gg 2$) hard X-ray indices. This would then imply that the hard X-ray continuum emission of radio-quiet quasars is different from Seyfert 1 galaxies and radio-loud quasars. Indeed, Seyfert 1s are constrained from *BeppoSAX* or *RXTE* to have hard X-ray indices in the range of $\Gamma = 1.6$ – 1.9 (e.g. Perola et al. 2002), as also found in radio-loud quasars, where $\Gamma \sim 1.7$ – 1.9 (Sambruna et al. 2002). For the radio-quiet quasars, this model can only be tested with high *S/N* data above 10 keV in order to measure the hard X-ray photon indices, which will be possible for example with the high sensitivity of the hard X-ray detector on the satellite *Astro-E2*.

8. Global properties and correlations

We now study the global properties of the present 21 quasars. For individual notes on each object, see Appendix A.

First, we focus on the mean photon index. In the 2–5 keV energy range, we find an average value of $\Gamma = 1.99$ with a standard deviation (σ) of 0.31 (see Table 11). We also calculate the mean photon index for each type of quasars present in the sample: NLG, RQQ, RLQ. The value found for RQQ is consistent with those found from *ASCA* data, i.e. $\Gamma = 1.78 \pm 0.11$ ($\sigma = 0.29^{+0.09}_{-0.07}$), and $\Gamma = 1.89 \pm 0.05$ (Leighly 1999; and Reeves & Turner 2000, respectively). NLG have the steepest power law index compared to optical broad line quasars, such as RQQ and RLQ (Table 11). This confirms previous results and is compatible with the photon index found with *ASCA*: 2.19 ± 0.10 ($\sigma = 0.30^{+0.07}_{-0.06}$), and 2.12 ($\sigma = 0.26$), by Leighly (1999) and Vaughan et al. (1999), respectively. The mean soft photon index (0.3–2 keV) is high with 2.56 (with a standard deviation of 0.44), consistent with *ROSAT* results ($\Gamma = 2.55 \pm 0.33$, Wang et al. 1996; $\Gamma = 2.58 \pm 0.05$ Yuan et al. 1998). For NLG the mean soft photon index is even higher with 3.04 ($\sigma = 0.42$) and consistent with the mean values of 3.29 ± 0.61 calculated by Wang et al. (1996) for objects exhibiting extreme Fe II emission (including I Zw 1, PG 1244+051, PG 1402+261, Mrk 478). The values reported in Table 11 strongly suggest that the steepest soft X-ray spectra correspond to the steepest hard X-ray spectra. This is confirmed below.

We now test some Spearman-rank correlations between the X-ray parameters ($\Gamma_{0.3-2}$, Γ_{2-5} , $L_{0.3-2}$, L_{2-10}), and some quasar characteristics: *FWHM*(H β), radio-loudness (R_L), the black hole mass (M_{BH}), and the accretion rate (\dot{m}). The results are reported in Table 12. We find a very strong anti-correlation between Γ_{2-5} , $\Gamma_{0.3-2}$ and the *FWHM*(H β) line (Fig. 3). This confirms the results found previously (e.g., Boller et al. 1996; Wang et al. 1996; Brandt et al. 1997; Vaughan et al. 1999; Reeves & Turner 2000; Dewangan 2002). Indeed spectra appear much softer in objects with narrow permitted optical H β lines. We find also a very significant correlation between $\Gamma_{0.3-2}$ and Γ_{2-5} (Fig. 3), meaning that a steep soft photon index leads to a steep hard photon index, consistent with Compton cooling models. Both, soft and hard photon index are strongly anti-correlated with the black hole mass, and positively correlated with the accretion rate relative to Eddington (Fig. 3). Thus the steepest objects have the lowest black hole masses and the highest accretion rates. Therefore, a high accretion rate and a smaller black hole mass is likely to be the physical driver responsible for these trends, leading to a higher inner disk temperature, which results in a stronger soft X-ray excess (and therefore a steeper soft photon index) and subsequently a steep hard power law.

9. Summary and conclusions

We have presented results from *XMM-Newton* EPIC observations of 21 low redshift quasars with redshifts less than 0.4. All objects are Palomar Green quasars and have low Galactic absorption along the line-of-sight. Five objects are Narrow Line Seyfert1/quasars, two are RLQ, and the other 14 objects are RQQ. We now summarize our main results:

About 90% of the present quasars (19/21) exhibit a significant soft excess at energies below about 1–1.5 keV. This result is in contrast to previous findings with *ASCA*, e.g.

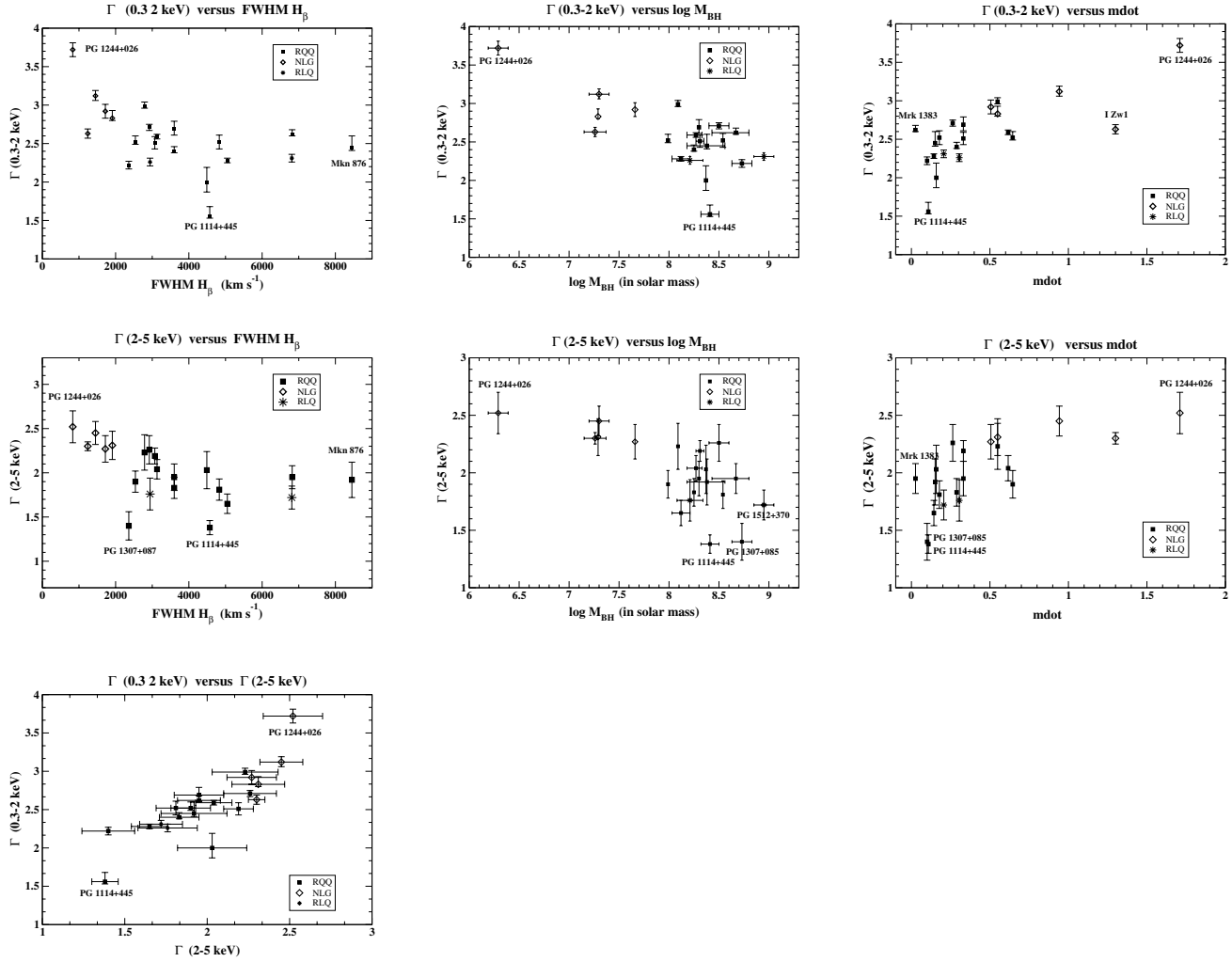


Fig. 3. Correlations between X-ray and AGN properties.

George et al. (2000) found that only five of their 14 PG quasars (with $z \leq 0.25$) require a soft excess below 1 keV. This is likely due to the smaller band-pass of *ASCA* compared to *XMM-Newton* at lower energies. For objects with a strong soft excess and a large Fe K line, the soft excess cannot be solely due to reprocessing of the primary X-ray component by an ionized disk. In all objects in the present sample (except possibly PG 1244+026), the soft X-ray excess is much better explained by Comptonization of soft photons in a hot plasma, than by the thermal emission from a thin standard accretion disk, as the inferred disc temperatures appear to be too hot. However, to definitely discriminate between these two models, a larger bandpass is required, from the EUV (for the soft component) to hard X-rays up to few 100 keV (for the hard component).

PG 1114+445 shows a huge absorption trough between 0.6 and 1.5 keV, due to the presence of a warm absorber. Fitting the spectrum with two absorption edges, we find very large optical depths of $\tau \sim 2.23$ and $\tau \sim 0.53$ at $E = 0.72$ keV and $E = 0.93$ keV, respectively. Further nine other objects show the presence of one or two absorption edges near those of O VII (0.74 keV) and O VIII (0.87 keV). This means that at least 50% of our present quasars show absorption, which is compatible with the fraction found in Seyfert 1 galaxies at lower redshift

(e.g., Reynolds 1997 with *ASCA*). This is the first time that such a high fraction of warm absorbers is found in quasars and may imply a similar covering fraction of the absorbing material compared to the Seyfert 1s. The lack of detection of warm absorbers in quasars with *ROSAT* and *ASCA* may have been due to the limited bandpass for both instruments, i.e. the lack of soft response of *ASCA* and the limited spectral resolution of the *ROSAT* PSPC. The present data do not enable us to determine the exact nature (ionization degree, velocity, etc.) and the complexity (e.g., absorption/emission lines, absorption edges) of the absorbing medium. Higher spectral resolution data are required (e.g. RGS), which will be investigated in a subsequent paper.

We find evidence for Fe K shell emission lines in at least twelve objects. Indeed, this is probably a lower limit on the number of objects with iron lines, since the line detection depends on the exposure times which are very short in some objects. Nonetheless, iron lines are detected in five objects at >99% confidence (IZw1, PG 0804+761, PG 1114+445, PG 1116+215 and PG 1402+261), whilst seven objects have a more marginal detection at 90–99% confidence (PG 0947+396, PG 1048+342, PG 1115+407, PG 1244+026, PG 1309+355, Mkn 1383, and PG 1512+370). In five objects the line energy

is consistent within the errors with 6.4 keV, a “neutral” to moderately ionized iron (i.e. $\leq \text{Fe XVII}$), while for the other seven objects the line energy is consistent with highly ionized iron: IZw1, PG 0804+761, PG 1115+407, PG 1116+215, PG 1244+026, PG 1402+261, and Mrk 1383. For five objects the fit is statistically improved when leaving the width of the line as a free parameter. All these line profiles can be well fitted with either a broad Gaussian line, or with a relativistic line profile (non-rotating Schwarzschild BH or rapidly rotating Kerr BH). No significant differences have been found comparing the χ^2 obtained for the relativistic line profile and for the broad Gaussian line. The width of the Gaussian line could be due to a blend of several (neutral/ionized) lines or simply to Keplerian motion. With the present *S/N* data we are not able to infer the incidence of genuine relativistic effects in quasars. Higher *S/N* data or larger spectral resolution are needed for such investigation. The line profiles can be also interpreted as ionized disk reflection, which is able to explain the spectral shape over the 2–12 keV energy range. At least five significant detections (at $\geq 99\%$ confidence) of broad iron lines in quasars have been found with *XMM-Newton* to date: IZw1, PG 0804+761, PG 1116+215, and PG 1402+261 (this work), and Q 0056+363 (Porquet et al. 2003). The first three objects exhibit line energies corresponding to very ionized iron (He-like, H-like). As shown previously by Porquet & Reeves (2003), broad and intense lines at 6.4 keV in quasars appear to be very rare, with the quasar Q0056-363 being the most luminous quasar found to date exhibiting such characteristics.

The RQQ PG 1402+261 shows a very large positive deviation near 7–8 keV compared to a power law model. Assuming that this feature is a relativistic Fe K line, we find a huge *EW* of about 2 keV, thus the hard X-ray spectrum of this object is likely to be dominated by reflected emission from the disc. Other interpretations such as partial covering absorber models will be investigated in detail in a forthcoming paper (Reeves et al. 2004). Four of the five NLG of the sample show the presence of a very highly ionized Fe K line: IZw1, PG 1115+407, PG 1244+026, and PG 1402+261. Our results are also consistent with the correlations found between the Fe K line energy and the 2–10 keV X-ray power law slope by Dewangan (2002). This means that the steep X-ray spectrum objects (such as NLG) tend to have Fe K lines formed in a highly ionized medium, while objects with flatter X-ray spectra tend to be associated with near neutral or weakly ionized iron line emission.

A strong correlation is found between Γ (both in the soft 0.3–2 keV and hard 2–10 keV energy bands) and optical $H\beta$ width, whereby the steepest X-ray spectra tend to be found in those objects with narrow $H\beta$ widths. This is consistent with previous results (e.g., Boller et al. 1996; Wang et al. 1996; Brandt et al. 1997; Vaughan et al. 1999; Reeves & Turner 2000; Dewangan 2002). The soft and hard X-ray photon indices are also linked by a very strong correlation, i.e. the steepest soft X-ray spectra lead to the steepest hard X-ray spectra. The strongest correlations are found between Γ (soft and hard), $H\beta$ width and the black hole mass and the accretion rate. Therefore, we conclude that a high accretion rate and a smaller black hole mass is likely to be the physical driver responsible for these trends, i.e. the steepest X-ray spectra are often found in objects

accreting at high fraction of the Eddington rate, with smaller black hole masses.

Acknowledgements. Based on observations obtained with the *XMM-Newton*, an ESA science mission with instruments and contributions directly funded by ESA member states and the USA (NASA). We would like to thank the anonymous referee for fruitful comments and suggestions. D.P. acknowledges grant support from an MPE fellowship.

References

- Anders, E., & Grevesse, N. 1989, *Geochim. Cosmochim. Acta*, 53, 197
- Arnaud, K.A., Branduardi-Raymont, G., Culhane, J. L., et al. 1985, *MNRAS*, 217, 105
- Behar, E., Sako, M., & Kahn, S. M. 2001, *ApJ*, 563, 497
- Bevington, P. R., & Robinson, D. K. 1992, *Data reduction and error analysis for the physical sciences* (New York: McGraw-Hill)
- Boller, T., Brandt, W. N., & Fink, H. 1996, *A&A*, 305, 53
- Boroson, T. A., & Green, R. F. 1992, *ApJS*, 80, 109
- Brandt, W. N., Mathur, S., & Elvis, M. 1997, *MNRAS*, 285, L25
- Brandt, W. N., Laor, A., & Wills, B. J. 2000, *ApJ*, 528, 637
- Brinkmann, W. 1992, in *X-ray Emission from Active Galactic Nuclei and the Cosmic X-ray Background*, ed. W. Brinkmann, & J. Truemper, MPE report 235, 143
- Brinkmann, W., Papadakis, I. E., & Ferrero, E. 2004a, *A&A*, 414, 107
- Brinkmann, W., Arevalo, P., Gliozzi, M., & Ferrero, E. 2004b, *A&A*, 415, 959
- Buehler, P., Courvoisier, T. J.-L., Staubert, R., et al. 1995, *A&A*, 295, 309
- Dewangan, G. C. 2002, *ApJ*, 581, L71
- Dickey, J. M., & Lockman, F. J. 1990, *ARA&A*, 28, 215
- Fabian, A. C., Rees, M. J., Stella, L., & White, N. E. 1989, *MNRAS*, 238, 729
- Fabian, A. C., Vaughan, S., Nandra, K., et al. 2002, *MNRAS*, 335, L1
- Ferrarese, L., Pogge, R. W., Peterson, B. M., et al. 2001, *ApJ*, 555, L79
- Fiore, F., Elvis, M., McDowell, J. C., et al. 1994, *ApJ*, 431, 515
- Fiore, F., Matt, G., & Cappi, M. 1998, *MNRAS*, 298, 103
- Gallo, L. C., Boller, Th., Brandt, W. N., et al. 2004, *A&A*, 417, 29
- George, I. M., Nandra, K., Laor, A., et al. 1997, *ApJ*, 491, 508
- George, I. M., Turner, T. J., Netzer, H., et al. 1998, *ApJS*, 114, 73
- George, I. M., Turner, T. J., Yaqoob, T., et al. 2000, *ApJ*, 531, 52
- Gierliński, M., Zdziarski, A. A., Poutanen, J., et al. 1999, *MNRAS*, 309, 496
- Gierliński, M., & Done, C. 2004, *MNRAS*, 349, L7
- Green, R. F., Schmidt, M., & Liebert, J. 1986, *ApJS*, 61, 305
- Grupe, D., Wills, B. J., Leighly, K. M., & Meusinger, H. 2004, *AJ*, 127, 156
- Halpern, J. P. 1984, *ApJ*, 281, 90
- Kaastra, J. S., Steenbrugge, K. C., Raassen, A. J. J., et al. 2002, *A&A*, 386, 427
- Kaspi, S., Smith, P. S., Netzer, H., et al. 2000, *ApJ*, 533, 631
- Kaspi, S., Brandt, W. N., Netzer, H., et al. 2001, *ApJ*, 554, 216
- Kellermann, K. I., Sramek, R., Schmidt, M., et al. 1989, *AJ*, 98, 1195
- Kinkhabwala, A., Sako, M., Behar, E., et al. 2002, *ApJ*, 575, 732
- Kirsch, M. 2003, EPIC status of calibration and data analysis, *XMM-SOC-CAL-TN-0018* (issue 2.1)
- Laor, A. 1991, *ApJ*, 376, 90
- Laor, A., Fiore, F., Elvis, M., et al. 1994, *ApJ*, 435, 611
- Laor, A., Fiore, F., Elvis, M., et al. 1997, *ApJ*, 477, 93
- Lawson, A. J., & Turner, M. J. L. 1997, *MNRAS*, 288, 920
- Leighly, K. M. 1999, *ApJS*, 125, 317

- Mathur, S., Wilkes, B., & Elvis, M. 1998, *ApJ*, 503, L23
- Malkan, M. A., & Sargent, W. L. W. 1982, *ApJ*, 254, 22
- Marshall, H. L., Edelson, R. A., Vaughan, S., et al. 2003, *AJ*, 125, 459
- Mineo, T., Fiore, F., Laor, A., et al. 2000, *A&A*, 359, 471
- Nandra, K., George, I. M., Turner, T. J., & Fukazawa, Y. 1996, *ApJ*, 464, 165
- Nayakshin, S., Kazanas, D., & Kallman, T. 2000, *ApJ*, 537, 833
- Netzer, H. 1996, *ApJ*, 473, 781
- O'Brien, P. T., Reeves, J. N., Turner, M. J. L., et al. 2001, *A&A*, 365, L122
- Page, K. L., Pounds, K. A., Reeves, J. N., & O'Brien, P. T. 2002, *MNRAS*, 330, L1
- Page, K. L., O'Brien, P. T., Reeves, J. N., & Breeveld, A. A. 2003, *MNRAS*, 340, 1052
- Page, K. L., O'Brien, P. T., Reeves, J. N., & Turner, M. J. L. 2004, *MNRAS*, 347, 316
- Papadakis, I. E., Reig, P., & Nandra, K. 2003, *MNRAS*, 344, 993
- Perola, G. C., Matt, G., Cappi, M., et al. 2002, *A&A*, 389, 802
- Peterson, B. M. 1997, *An introduction to active galactic nuclei* (New York: Cambridge University Press)
- Porquet, D., Dumont, A.-M., Collin, S., & Mouchet, M. 1999, *A&A*, 341, 58
- Porquet, D., & Reeves, J. N. 2003, *A&A*, 408, 119
- Pounds, K., Reeves, J., O'Brien, P., Page, K., et al. 2001, *ApJ*, 559, 181
- Pounds, K., & Reeves, J. 2002, *New Visions of the X-ray Universe in the XMM-Newton and Chandra Era*, in press [arXiv:astro-ph/0201436]
- Reeves, J. N., & Turner, M. J. L. 2000, *MNRAS*, 316, 234
- Reeves, J. N., Turner, M. J. L., Pounds, K. A., et al. 2001, *A&A*, 365, L134
- Reeves, J. N., O'Brien, P. T., & Ward, M. J. 2003, *ApJ*, 593, L65
- Reeves, J. N., Porquet, D., & Turner, T. J. 2004, *ApJL*, submitted
- Ross, R. R., Fabian, A. C., & Young, A. J. 1999, *MNRAS*, 306, 461
- Reynolds, C. S., & Fabian, A. C. 1995, *MNRAS*, 273, 1167
- Reynolds, C. S. 1997, *MNRAS*, 286, 513
- Sako, M., Kahn, S. M., Behar, E., et al. 2001, *A&A*, 365, L168
- Sambruna, R. M., Eracleous, M., & Mushotzky, R. F. 2002, *New Astron. Rev.*, 46, 215
- Schmidt, M., & Green, R. F. 1983, *ApJ*, 269, 352
- Shields, G. A., Gebhardt, K., Salviander, S., et al. 2003, *ApJ*, 583, 124
- Strüder, L., Briel, U., Dennerl, K., et al. 2001, *A&A*, 365, L5
- Tanaka, Y., Nandra, K., & Fabian, A. C., et al. 1995, *Nature*, 375, 659
- Titarchuk, L. 1994, *ApJ*, 434, 570
- Titarchuk, L., & Lyubarskij, Y. 1995, *ApJ*, 450, 876
- Turner, T. J., & Pounds, K. A. 1989, *MNRAS*, 240, 833
- Turner, M. J. L., Abbey, A., Arnaud, M., et al. 2001, *A&A*, 365, L27
- Vaughan, S., Reeves, J., Warwick, R., & Edelson, R. 1999, *MNRAS*, 309, 113
- Vestergaard, M. 2002, *ApJ*, 571, 733
- Wang, T., Brinkmann, W., & Bergeron, J. 1996, *A&A*, 309, 81
- Wilms, J., Allen, A., & McCray, R. 2000, *ApJ*, 542, 914
- Woo, J., & Urry, C. M. 2002, *ApJ*, 579, 530
- Yaqoob, T., George, I. M., Nandra, K., et al. 2001, *ApJ*, 546, 759
- Yuan, W., Brinkmann, W., Siebert, J., & Voges, W. 1998, *A&A*, 330, 108

Online Material

Table 2. List of the *XMM-Newton* observations. Column (1): Name of the source; Col. (2): observation date (dd/mm/yyyy), Col. (3): orbit revolution number, Col. (4): Observation ID, and Col. (5): data exposure time of the pn data (in ks), except for PG 0804+761 for which the MOS exposure time is given.

Source	Obs. Date	Rev.	Obs-ID	Exp.
IZw1	22/06/2002	464	0110890301	18.7
PG 0804+761	04/04/2000	166	0102040401	6.7
PG 0947+396	03/11/2001	349	0111290101	17.6
PG 0953+414	22/11/2001	358	0111290201	11.5
PG 1048+342	13/05/2002	444	0109080701	28.1
PG 1114+445	14/05/2002	445	0109080801	35.0
PG 1115+407	02/12/2001	446	0111290301	15.0
PG 1116+215	02/12/2001	363	0111290401	5.5
PG 1202+281	30/05/2002	453	0109080101	12.0
PG 1244+026	17/06/2001	279	0051760101	7.2
PG 1307+085	13/06/2002	460	0110950401	11.2
PG 1309+355	10/06/2002	458	0109080201	22.3
PG 1322+659	11/05/2002	443	0109080301	8.7
PG 1352+183	20/07/2002	478	0109080401	12.5
PG 1402+261	27/02/2002	391	0109081001	9.1
Mrk 1383	28/07/2000	116	0102040501	5.4
PG 1427+480	31/05/2002	453	0109080901	31.2
Mrk 478	23/12/2001	373	0107660201	9.1
PG 1512+370	25/08/2002	496	0111291001	17.6
Mrk 876	29/08/2001	315	0102041301	2.5
PG 1626+554	05/05/2002	440	0109081101	5.5

Table 3. Black hole mass (M_{BH}), monochromatic luminosity $\nu L_{\nu}(5100 \text{ \AA})$, bolometric luminosity (L_{bol}), and accretion rate with respect to Eddington. (*) $L_{\text{bol}} \simeq 9 \times \nu L_{\nu}(5100 \text{ \AA})$. (**) using the relation (3) given by Woo & Urry et al. (2002) between M_{BH} and $\nu L_{\nu}(5100 \text{ \AA})$. (^a) Kaspi et al. (2000), (^b) Vestergaard (2002), and (^c) Shields et al. (2003), (^d) Grupe et al. (2004), and (^e) Woo & Urry (2002).

Source	$\log M_{\text{BH}}$ (M_{\odot})	$\log \nu L_{\nu}(5100\text{\AA})$ (erg s^{-1})	$\log L_{\text{bol}}$ (erg s^{-1})	\dot{m}
I Zw1	$7.26 \pm 0.11^{(b)}$	$44.52 \pm 0.12^{(b)}$	$45.47 \pm 0.12^{(*)}$	1.30
PG 0804+761	$8.31 \pm 0.04^{(a)}$	$44.82^{+0.07(a)}_{-0.09}$	$45.93^{(e)}$	0.33
PG 0947+396	$8.54^{(c)}$	$44.94^{(c)}$	$45.89^{(*)}$	0.18
PG 0953+414	$8.27^{+0.06(a)}_{-0.09}$	$45.08^{+0.05(a)}_{-0.07}$	$46.16^{(e)}$	0.62
PG 1048+342	$8.25^{(c)}$	$44.86^{(c)}$	$45.81^{(*)}$	0.29
PG 1114+445	$8.41 \pm 0.09^{(b)}$	$44.59 \pm 0.07^{(b)}$	$45.54^{(*)}$	0.11
PG 1115+407	$7.66^{(**)}$	$44.51^{(d)}$	$45.83^{(d)}$	0.51
PG 1116+215	$8.50 \pm 0.10^{(b)}$	$45.27 \pm 0.07^{(b)}$	$46.02^{(e)}$	0.26
PG 1202+281	$8.12 \pm 0.09^{(b)}$	$44.42 \pm 0.07^{(b)}$	$45.26^{(d)}$	0.14
PG 1244+026	$6.29 \pm 0.10^{(b)}$	$43.67 \pm 0.08^{(b)}$	$44.75^{(d)}$	1.71
PG 1307+085	$8.73 \pm 0.10^{(b)}$	$44.86 \pm 0.07^{(b)}$	$45.83^{(e)}$	0.10
PG 1309+355	$8.21 \pm 0.13^{(b)}$	$44.84 \pm 0.07^{(b)}$	$45.82 \pm 0.07^{(*)}$	0.31
PG 1322+659	$8.09^{(c)}$	$44.98^{(c)}$	$45.93^{(*)}$	0.55
PG 1352+183	$8.30^{(c)}$	$44.97^{(c)}$	$45.92^{(*)}$	0.33
PG 1402+261	$7.29^{(e)}$		$45.13^{(e)}$	0.55
Mrk 1383	$8.67^{+0.13(a)}_{-0.24}$	$44.61^{+0.06(a)}_{-0.07}$	$45.19^{(e)}$	0.03
PG 1427+480	$7.99^{(c)}$	$44.95^{(c)}$	$45.90^{(*)}$	0.65
Mrk 478	$7.30 \pm 0.10^{(b)}$	$44.42 \pm 0.07^{(b)}$	$45.88^{(d)}$	0.94
PG 1512+370	$8.95 \pm 0.10^{(b)}$	$45.41 \pm 0.06^{(b)}$	$46.36 \pm 0.06^{(*)}$	0.21
Mrk 876	$8.38^{+0.18(a)}_{-0.20}$	$44.84 \pm 0.06^{(a)}$	$45.66^{(e)}$	0.15
PG 1626+554	$8.37^{(c)}$	$44.72^{(c)}$	$45.67^{(d)}$	0.16

Table 4. Spectral fits with an absorbed power law continuum in two energy bands (2–5 keV and 0.3–2 keV). Galactic absorption ($N_{\text{H}}^{\text{Gal}}$) and intrinsic absorption (N_{H}^{in}) of the QSO in its rest frame are expressed in 10^{20} cm^{-2} . (^a) absorption edge(s) added to the continuum model (see parameter values in Table 6).

Source	$N_{\text{H}}^{\text{Gal}}$	Γ_{2-5}	$\chi^2/\text{d.o.f.}$	$P(\chi^2)$	N_{H}^{in}	$\Gamma_{0.3-2}$	$\chi^2/\text{d.o.f.}$	$P(\chi^2)$
I Zw1	4.94	2.30 ± 0.05	167.4/132	2.0	^(a) 7.8 ± 1.0	2.63 ± 0.06	352.8/324	13.0
PG 0804+761	3.01	2.19 ± 0.09	161.5/196	96.6	^(a) 2.3 ± 1.1	2.51 ± 0.08	248.6/220	9.0
PG 0947+396	1.55	1.81 ± 0.12	128.3/122	33.1	^(a) 2.1 ± 1.4	2.52 ± 0.09	285.1/312	86.0
PG 0953+414	0.82	2.04 ± 0.11	55.7/75	95.2	<0.4	2.59 ± 0.03	337.0/278	0.9
PG 1048+342	1.94	1.83 ± 0.12	85.8/81	33.7	<0.8	$2.40^{+0.06}_{-0.02}$	239.3/267	8.5
PG 1114+445	1.62	1.38 ± 0.08	123.3/131	67.2	^(a) <2.0	$1.56^{+0.12}_{-0.03}$	267.9/213	0.6
PG 1115+407	1.91	2.27 ± 0.15	58.9/81	96.9	^(a) $2.1^{+1.7}_{-1.3}$	2.92 ± 0.09	268.0/300	90.8
PG 1116+215	1.29	2.26 ± 0.16	98.6/80	7.8	<0.5	2.71 ± 0.04	263.6/294	89.8
PG 1202+281	1.70	1.65 ± 0.11	68.9/78	76.0	^(a) <0.3	2.28 ± 0.03	309.9/264	2.7
PG 1244+026	1.78	2.52 ± 0.18	96.5/79	8.8	11.5 ± 0.1	3.72 ± 0.09	407.6/296	0
PG 1307+085	2.10	1.40 ± 0.16	74.5/81	68.3	^(a) <0.3	2.22 ± 0.05	268.8/219	1.2
PG 1309+355	1.02	1.76 ± 0.18	51.8/62	81.8	^(a) <0.5	2.26 ± 0.05	197.8/212	75.0
PG 1322+659	2.00	2.23 ± 0.20	52.8/57	63.2	<0.7	$2.99^{+0.05}_{-0.03}$	275.6/257	20.3
PG 1352+183	2.05	1.95 ± 0.15	126.2/107	9.9	^(a) <2.3	$2.69^{+0.10}_{-0.08}$	311.9/299	29.2
PG 1402+261	1.47	2.31 ± 0.16	75.5/73	39.8	<1.5	$2.83^{+0.10}_{-0.03}$	319.4/288	9.8
Mrk 1383	2.85	1.95 ± 0.13	92.9/110	87.9	<0.8	$2.62^{+0.06}_{-0.02}$	321.2/313	36.2
PG 1427+480	1.86	1.90 ± 0.12	104.3/123	90.0	<1.4	$2.52^{+0.08}_{-0.03}$	344.1/311	9.5
Mrk 478	1.04	2.45 ± 0.13	90.9/115	95.2	0.9 ± 0.8	$3.12^{+0.07}_{-0.06}$	322.7/319	43.2
PG 1512+370	1.35	1.72 ± 0.13	125.0/124	45.8	<0.8	2.31 ± 0.04	301.4/305	54.7
Mrk 876	2.85	1.92 ± 0.20	47.2/61	90.2	^(a) <2.3	$2.45^{+0.15}_{-0.04}$	254.2/230	13.1
PG 1626+554	2.02	2.03 ± 0.21	61.2/82	95.8	<0.7	$2.00^{+0.19}_{-0.13}$	96.9/122	95.4

Table 5. Spectral fit with a broken power law model (Γ_{soft} , Γ_{hard} , and E_c break point for the energy in keV), including the Galactic ($N_{\text{H}}^{\text{Gal}}$) and intrinsic (N_{H}^{in}) absorptions (expressed in 10^{20} cm^{-2}). The unabsorbed fluxes are expressed in $10^{-12} \text{ erg s}^{-1} \text{ cm}^{-2}$. In parentheses are reported the luminosities (expressed in $10^{44} \text{ erg s}^{-1}$). The last column reports the flux ratio in the 0.3–2 keV and 0.3–10 keV energy bands. For PG 1114+445, two strong absorption edges are required (see values in Table 6).

Source	N_{H}^{in}	Γ_{soft}	Γ_{hard}	E_c	$\chi^2/\text{d.o.f.}$	$P(\chi^2)$	$F_{0.3-10} (L)$	$F_{2-10} (L)$	$\frac{0.3-2 \text{ keV}}{0.3-10 \text{ keV}}$
IZw1	5.0 ± 0.6	2.61 ± 0.10	2.37 ± 0.02	0.67 ± 0.05	642.0/495	0	28.3 (2.1)	8.4 (0.63)	70%
PG 0804+761	<2.8	$2.47^{+0.19}_{-0.10}$	$2.16^{+0.04}_{-0.09}$	$1.26^{+0.50}_{-0.12}$	489.0/475	31.8	32. (6.6)	11. (2.2)	66%
PG 0947+396	<0.7	2.41 ± 0.03	1.75 ± 0.09	2.28 ± 0.23	462.9/484	74.8	4.6 (4.3)	1.8 (1.5)	61%
PG 0953+414	<0.6	$2.60^{+0.05}_{-0.02}$	2.02 ± 0.07	1.77 ± 0.19	410.9/380	13.2	9.3 (12.3)	3.0 (3.7)	68%
PG 1048+342	<1.2	$2.40^{+0.11}_{-0.03}$	1.80 ± 0.07	$1.80^{+0.21}_{-0.17}$	428.3/386	6.8	3.3 (1.9)	1.4 (0.76)	58%
PG 1114+445	<1.5	$1.56^{+0.09}_{-0.04}$	1.53 ± 0.03	2.0 (f)	481.4/410	0.9	3.1 (1.2)	2.3 (0.89)	26%
PG 1115+407	<0.8	$2.85^{+0.06}_{-0.02}$	2.19 ± 0.10	$2.04^{+0.24}_{-0.20}$	357.0/406	96.2	5.3 (2.9)	1.2 (0.60)	77%
PG 1116+215	<1.9	$2.72^{+0.18}_{-0.03}$	2.17 ± 0.11	$1.76^{+0.32}_{-0.41}$	396.3/401	55.7	12. (8.3)	3.2 (2.1)	73%
PG 1202+281	<0.5	2.29 ± 0.04	1.71 ± 0.06	$1.76^{+0.24}_{-0.16}$	413.8/375	8.2	7.8 (4.4)	3.6 (1.9)	55%
PG 1244+026	12.1 ± 0.1	3.77 ± 0.11	2.51 ± 0.10	$1.81^{+0.12}_{-0.09}$	523.8/403	0	29. (1.4)	2.2 (0.099)	92%
PG 1307+085	<7.0	$2.86^{+0.47}_{-0.22}$	1.52 ± 0.06	0.93 ± 0.06	360.4/338	19.3	3.4 (1.7)	1.9 (0.87)	44%
PG 1309+355	<3.4	$2.92^{+0.34}_{-0.13}$	1.73 ± 0.05	0.78 ± 0.05	269.1/301	90.7	1.4 (1.0)	0.71 (0.48)	49%
PG 1322+659	<2.8	$3.01^{+0.24}_{-0.04}$	$2.18^{+0.14}_{+0.11}$	$1.62^{+0.19}_{-0.25}$	337.3/336	47.0	5.8 (3.8)	1.3 (0.77)	78%
PG 1352+183	<0.7	2.65 ± 0.04	1.93 ± 0.10	$2.00^{+0.17}_{-0.23}$	485.2/458	18.3	6.0 (3.0)	1.9 (0.88)	68%
PG 1402+261	<2.8	$2.91^{+0.13}_{-0.09}$	$2.18^{+0.08}_{-0.13}$	$1.73^{+0.35}_{-0.17}$	424.1/384	7.7	7.7 (4.7)	1.8 (1.0)	77%
Mrk 1383	<1.2	$2.62^{+0.11}_{-0.02}$	1.96 ± 0.10	$1.91^{+0.25}_{-0.28}$	457.4/460	52.6	23. (3.6)	7.5 (1.1)	67%
PG 1427+480	<1.6	$2.53^{+0.10}_{-0.03}$	1.87 ± 0.07	$1.92^{+0.17}_{-0.22}$	495.5/488	39.8	2.8 (3.0)	1.0 (1.0)	64%
Mrk 478	2.2 ± 1.1	3.25 ± 0.10	2.38 ± 0.06	1.56 ± 0.10	422.3/465	92.2	17. (2.2)	2.7 (0.33)	84%
PG 1512+370	<0.9	2.31 ± 0.04	1.78 ± 0.05	$1.81^{+0.16}_{-0.13}$	473.1/479	56.7	4.3 (13.)	1.9 (5.3)	56%
Mrk 876	<2.3	$2.56^{+0.19}_{-0.06}$	$1.85^{+0.08}_{-0.10}$	$1.45^{+0.21}_{-0.13}$	344.6/322	18.5	12.9 (4.5)	5.2 (1.7)	60%
PG 1626+554	<0.8	2.41 ± 0.05	1.99 ± 0.12	$1.72^{+0.43}_{-0.52}$	388.0/388	49.0	8.3 (3.0)	3.1 (1.1)	63%

Table 6. Spectral fit of absorption edge(s). τ is the optical depth. Significant detections ($\geq 99\%$) are marked in bold face.

Object	τ_{OVII}	τ_{OVIII}	Detection	Edge parameters		Detection
	($E = 0.74 \text{ keV}$)	($E = 0.87 \text{ keV}$)		E (keV)	τ	
IZw1	0.11 ± 0.04	<0.01	99.9%	0.65 ± 0.02	0.21 ± 0.04	>99.99%
PG 0804+761	<0.09	0.07 ± 0.06	90.3%	0.62 ± 0.04	0.16 ± 0.09	99.2%
				0.95 ± 0.05	0.13 ± 0.06	
PG 0947+396	<0.10	0.15 ± 0.08	99.8%	0.85 ± 0.04	0.16 ± 0.08	99.9%
PG 1114+445	$2.26^{+0.22}_{-0.19}$	0.32 ± 0.16	>99.99%	0.72 ± 0.01	2.23 ± 0.17	>99.99%
				0.93 ± 0.03	0.53 ± 0.13	
PG 1115+407	<0.19	0.08 ± 0.06	91.8%	0.78 ± 0.05	0.15 ± 0.08	99.4%
				1.18 ± 0.10	0.15 ± 0.07	
PG 1116+215	<0.19	0.09 ± 0.07	97.7%			
PG 1202+281	0.09 ± 0.07	<0.13	99.9%	0.80 ± 0.05	0.13 ± 0.07	99.92%
PG 1307+085	$0.33^{+0.20}_{-0.16}$	<0.44	99.97%	0.78 ± 0.04	0.39 ± 0.16	99.97%
PG 1309+355	$0.46^{+0.20}_{-0.15}$	<0.25	99.98%	0.75 ± 0.03	0.49 ± 0.17	99.97%
PG 1352+183	0.11 ± 0.08	<0.08	97.0%	0.72 ± 0.06	0.12 ± 0.08	99.7%
Mrk 876	<0.23	0.25 ± 0.12	99.92%	0.93 ± 0.05	0.26 ± 0.11	99.97%

Table 7. Best-fitting spectral parameters for objects presenting a significant line detection (i.e. $P_{\text{prob}} \geq 90\%$). GA: Gaussian profile. D (DISKLINE) and L (LAOR): profile line emitted by a relativistic accretion disk for a non-rotating BH (Fabian et al. 1989) and a maximally rotating BH (Laor 1991), respectively. The inclination of the disk is fixed to 30 deg. We assume $q = -2$ (emissivity law), (*) for PG 1402+261 q is let as a free parameter: $|q| > 3.0$, and $|q| = 3.3^{+0.3}_{-0.5}$, respectively for D and L. D: $R_{\text{in}} = 6 R_g$ and $R_{\text{out}} = 1000 R_g$. L: $R_{\text{in}} = 1.26 R_g$, $R_{\text{out}} = 400 R_g$.

Object	Line	Line parameters			$P_{\text{prob}}^{\text{line}}$ (%)	$P_{\text{prob}}^{\text{broad}}$ (%)
		E (keV)	σ (keV)	EW (eV)		
IZw1	GA	$6.89^{+0.10}_{-0.15}$	0.01 (f)	69 ± 35	99.2	
	GA	$6.58^{+0.25}_{-0.37}$	$0.60^{+0.52}_{-0.30}$	297^{+240}_{-141}	>99.9	99.8
	D	6.78 ± 0.13		180 ± 68	>99.9	
	L	6.74 ± 0.11		240 ± 86	>99.9	
PG 0804+761	GA	6.76 ± 0.06	0.01 (f)	140^{+78}_{-76}	98.5	
	GA	$6.67^{+0.31}_{-0.37}$	$0.56^{+0.55}_{-0.22}$	482^{+356}_{-243}	99.7	98.4
	D	$6.82^{+0.16}_{-0.27}$		320^{+151}_{-156}	99.6	
	L	$6.71^{+0.27}_{-0.17}$		400^{+174}_{-180}	99.8	
PG 0947+396	GA	$6.45^{+0.07}_{-0.12}$	0.01 (f)	92 ± 65	94.9	
PG 1048+342	GA	$6.35^{+0.07}_{-0.10}$	0.01 (f)	123 ± 64	98.3	
PG 1114+445	GA	$6.40^{+0.02}_{-0.05}$	0.01 (f)	125 ± 41	>99.9	
PG 1115+407	GA	$7.20^{+0.13}_{-0.45}$	0.01 (f)	157^{+115}_{-125}	92.4	
PG 1116+215	GA	$7.23^{+0.07}_{-0.30}$	0.01 (f)	194 ± 123	96.3	
	GA	$6.67^{+0.36}_{-0.41}$	$0.72^{+0.48}_{-0.31}$	885^{+563}_{-213}	99.8	99.7
	D	$7.10^{+0.14}_{-0.16}$		517^{+251}_{-237}	99.8	
	L	7.06 ± 0.18		636^{+306}_{-285}	99.9	
PG 1244+026	GA	$6.66^{+0.09}_{-0.07}$	0.01 (f)	222 ± 156	92.4	
PG 1309+355	GA	$6.40^{+0.10}_{-0.12}$	0.01 (f)	156^{+100}_{-104}	97.4	
	GA	$6.48^{+0.18}_{-0.23}$	$0.21^{+0.24}_{-0.10}$	300^{+206}_{-173}	98.7	94.1
	D	$6.54^{+0.10}_{-0.16}$		373^{+187}_{-192}	99.8	
	L	$6.51^{+0.11}_{-0.15}$		458 ± 237	99.7	
PG 1402+261	GA	$7.38^{+0.07}_{-0.10}$	0.01 (f)	262^{+139}_{-140}	98.5	
	GA	$7.26^{+0.44}_{-0.51}$	$1.18^{+0.63}_{-0.40}$	2040^{+1340}_{-880}	>99.9	>99.9
	D(*)	$8.65^{+0.53}_{-0.37}$		2000^{+700}_{-780}	>99.9	
	L(*)	$8.51^{+0.33}_{-0.24}$		4460^{+2050}_{-1820}	>99.9	
Mrk 1383	GA	$6.62^{+0.12}_{-0.10}$	0.01 (f)	107^{+72}_{-81}	91.5	
PG 1512+370	GA	6.51 ± 0.13	0.01 (f)	93 ± 64	94.4	

Table 8. Fit results, in the 2–12 keV energy band, of a disk reflection model assuming a LAMPOST geometry for IZw1, PG 0804+761, PG 1114+445, PG 1116+215 and PG 1309+355, i.e. we assume a height of $10 R_g$, a ratio of X-ray to disk flux of 0.2 (with solar iron abundance). For PG 1402+261, a lower height above the AD of about $2.5 R_g$, an iron abundance of 5 relative to solar abundance are required. Its spectrum is dominated by reflection.

Object	Γ	θ (deg)	$r_{\text{in}} (r_g)$	$\chi^2/\text{d.o.f.}$
IZw1	2.28 ± 0.03	42^{+23}_{-19}	16^{+17}_{-10}	598.7/590
PG 0804+761	2.07 ± 0.06	42 ± 21	<14	212.2/250
PG 1116+215	2.12 ± 0.09	30 ± 22	<13	124.6/104
PG 1309+355	1.74 ± 0.09	<27	<30	62.9/86
PG 1402+261	2.13 ± 0.10	>60	<5	85.9/92

Table 9. Spectral fit with an absorbed black body spectrum of an accretion disk (DISKPN, kT_{diskpn}) combined with a power law model. $T_{\text{disk}}^{\text{max}}$ (in eV) represents the maximal values of the disk temperature for a standard α thin accretion disk at $3R_S$. kT_{diskpn} is expressed in eV. ^(a) one or two absorption edges are added to the continuum model due to the presence of a WA. ^(b) a Fe K line is added (either a Gaussian line or a LAOR line).

Source	$T_{\text{disk}}^{\text{max}}$	kT_{diskpn}	Γ	$\chi^2/\text{d.o.f.}$
IZw1 ^(a,b)	39	200 ± 25	2.33 ± 0.03	540.0/493
PG 0804+761 ^(a,b)	15	159 ⁺³⁰ ₋₂₃	2.22 ± 0.07	464.1/468
PG 0947+396 ^(a,b)	11	241 ± 15	1.88 ± 0.06	451.0/480
PG 0953+414	18	174 ± 8	2.12 ± 0.04	421.9/380
PG 1048+342 ^(b)	15	183 ± 11	1.91 ± 0.05	423.2/384
PG 1115+407 ^(a,b)	24	172 ± 14	2.40 ± 0.07	353.1/402
PG 1116+215 ^(a,b)	13	175 ⁺¹⁷ ₋₂₆	2.30 ± 0.07	375.8/397
PG 1202+281 ^(a)	14	223 ⁺¹⁴ ₋₁₇	1.72 ± 0.05	396.4/373
PG 1244+026 ^(b)	73	197 ± 11	2.39 ± 0.10	427.5/401
PG 1307+085 ^(a)	9	142 ⁺⁴¹ ₋₁₉	1.55 ± 0.07	338.6/336
PG 1309+355 ^(a,b)	16	144 ⁺³⁹ ₋₂₆	1.78 ± 0.08	244.4/296
PG 1322+659	19	149 ± 8	2.28 ± 0.07	226.3/336
PG 1352+183 ^(a)	15	201 ± 12	2.04 ± 0.08	478.8/456
PG 1402+261 ^(b)	31	151 ⁺¹¹ ₋₁₇	2.53 ± 0.09	400.4/381
Mrk 1383 ^(b)	7	160 ± 8	2.09 ± 0.05	442.8/458
PG 1427+480	21	190 ± 9	1.98 ± 0.05	505.9/488
Mrk 478	35	138 ± 4	2.48 ± 0.05	455.0/465
PG 1512+370 ^(b)	9	210 ± 19	1.90 ± 0.05	490.7/477
Mrk 876 ^(a)	9	177 ± 24	1.87 ± 0.11	326.9/320
PG 1626+554	12	145 ⁺²² ₋₂₄	2.09 ± 0.07	388.5/388

Table 10. Spectral fit with absorbed compTT+power law. For the COMP TT component model, the soft photon temperature (kT_1^{photon}) is fixed to T_{max} (Col. 1 of Table 9). kT^{plasma} is expressed in keV. τ corresponds to the plasma optical depth. The fits include the Galactic ($N_{\text{H}}^{\text{Gal}}$) and intrinsic (N_{H}^{in}) absorptions. Column densities are expressed in 10^{20} cm^{-2} . The unabsorbed fluxes are expressed in $10^{-12} \text{ erg s}^{-1} \text{ cm}^{-2}$. In parentheses are reported the luminosities (expressed in $10^{44} \text{ erg s}^{-1}$). The last column reports the flux ratio in the 0.3–2 keV and 0.3–10 keV energy bands. ^(a) one or two absorption edges are added to the continuum model due to the presence of a WA. ^(b) a Fe K line is added (either a Gaussian line or a LAOR line).

Source	N_{H}^{in}	kT^{plasma}	τ_1	Γ	$\chi^2/\text{d.o.f.}$	$F_{0.3-10}$ (L)	F_{2-10} (L)	$\frac{0.3-2 \text{ keV}}{0.3-10 \text{ keV}}$
IZw1 ^(a,b)	10.5 ± 2.6	0.22 ± 0.05	14.7 ^{+2.2} _{-1.3}	2.33 ± 0.03	525.7/490	36.3 (2.8)	8.6 (0.64)	76%
PG 0804+761 ^(a,b)	3.9 ^{+7.2} _{-3.1}	2.8 ^{+3.1} _{-1.4}	3.5 ^{+2.1} _{-1.1}	1.53 ^{+0.32} _{-0.17}	462.5/470	30.5 (6.1)	11.4 (2.3)	63%
PG 0947+396 ^(a,b)	<3.3	0.32 ± 0.06	15.6 ^{+0.8} _{-2.0}	1.76 ± 0.07	440.1/479	4.6 (4.2)	1.8 (1.6)	61%
PG 0953+414	<2.0	0.29 ^{+0.10} _{-0.06}	13.8 ^{+0.5} _{-1.0}	1.98 ± 0.05	408.6/379	9.1 (11.9)	3.0 (3.7)	67%
PG 1048+342 ^(b)	<1.8	0.25 ^{+0.09} _{-0.06}	16.6 ^{+0.8} _{-1.5}	1.82 ± 0.06	417.4/383	3.2 (1.9)	1.3 (0.74)	60%
PG 1114+445 ^(a,b)	5.2 ^{+2.5} _{-3.5}	3.1 ^{+9.7} _{-2.2}	6.7 ^{+3.2} _{-4.0}	1.51 (f)	214.6/236	3.3 (1.3)	2.3 (0.92)	30%
PG 1115+407 ^(a,b)	<7.2	0.17 ^{+0.08} _{-0.04}	19.2 ^{+5.4} _{-3.4}	2.40 ± 0.06	333.2/399	5.8 (3.1)	1.2 (0.60)	79%
PG 1116+215 ^(a,b)	<11.8	0.25 ^{+0.18} _{-0.07}	13.1 ^{+3.7} _{-2.1}	2.23 ± 0.08	370.3/396	14.8 (11.0)	3.2 (2.1)	78%
PG 1202+281 ^(a)	<6.7	0.24 ± 0.07	21.2 ^{+1.8} _{-4.8}	1.68 ± 0.04	396.9/372	7.5 (4.2)	3.6 (1.9)	52%
PG 1244+026 ^(b)	<2.1	0.18 ± 0.02	28.7 ^{+2.5} _{-4.0}	2.40 ± 0.08	426.8/400	12.4 (0.57)	2.1 (0.098)	83%
PG 1307+085 ^(a)	5.4 ± 4.2	0.10 ± 0.02	>44	1.46 ± 0.03	350.1/337	3.4 (1.6)	1.9 (0.87)	44%
PG 1309+355 ^(a,b)	<13.1	0.13 ^{+0.08} _{-0.03}	>23.4	1.78 ^{+0.09} _{-0.06}	244.4/295	1.4 (1.0)	0.72 (0.48)	49%
PG 1322+659	<4.3	0.17 ± 0.05	22.4 ^{+1.7} _{-3.7}	2.21 ± 0.07	327.1/335	5.3 (3.4)	1.3 (0.77)	76%
PG 1352+183 ^(a)	<6.8	0.25 ± 0.06	17.6 ^{+0.9} _{-3.0}	1.90 ± 0.08	476.0/455	5.7 (2.8)	1.9 (0.88)	67%
PG 1402+261 ^(b)	<3.1	0.25 ^{+0.11} _{-0.06}	14.2 ^{+0.6} _{-1.7}	2.20 ± 0.08	407.5/381	7.3 (4.4)	1.8 (1.0)	75%
Mrk 1383 ^(b)	<1.0	0.20 ± 0.05	19.1 ^{+0.9} _{-1.2}	2.02 ± 0.05	438.8/457	23.2 (3.5)	7.5 (1.1)	68%
PG 1427+480	<4.8	0.27 ^{+0.08} _{-0.05}	16.0 ^{+0.7} _{-2.4}	1.86 ± 0.05	494.9/487	2.7 (2.8)	1.0 (1.0)	63%
Mrk 478	<5.1	0.22 ± 0.05	13.6 ± 1.3	2.29 ± 0.06	416.4/464	15.8 (2.0)	2.7 (0.33)	83%
PG 1512+370 ^(b)	<6.5	0.44 ^{+0.72} _{-0.12}	10.9 ^{+0.6} _{-2.4}	1.74 ± 0.08	468.6/476	4.3 (13.5)	1.9 (5.4)	56%
Mrk 876 ^(a)	<4.0	0.14 ± 0.06	>37.4	1.86 ± 0.06	327.4/320	11.8 (4.0)	5.1 (1.7)	57%
PG 1626+554	<6.9	0.52 ^{+7.84} _{-0.30}	9.4 ^{+0.7} _{-2.2}	1.85 ± 0.17	385.9/387	8.0 (2.9)	3.1 (1.1)	61%

Table 11. Mean and standard deviation (σ) of the photon index in the 0.3–2 keV and 2–5 keV energy ranges. NLG: Narrow Line Galaxies ($FWHM < 2000 \text{ km s}^{-1}$), RQQ: radio-quiet quasars, and RLQ (radio-loud quasars).

Type	0.3–2 keV	2–5 keV
All objects	2.56 (σ :0.44)	1.99 (σ :0.31)
NLG	3.04 (σ :0.42)	2.37 (σ :0.11)
RQQ	2.43 (σ :0.35)	1.90 (σ :0.27)
RLQ	2.29 (σ :0.04)	1.74 (σ :0.03)

Table 12. Spearman-rank correlations. (r_s , P_{rs}): r_s Spearman coefficient, and P_{rs} probability. $r_s > 0$ and $r_s < 0$ means a correlation and an anti-correlation, respectively. Significant correlations ($\geq 99\%$) are marked in bold face.

	Γ_{2-5}	$L(2-10)$	$\Gamma_{0.3-2}$	$L(0.3-2)$	z	$FWHM$
$L(2-10)$	(-0.31, 83.6)	–	–	–	–	–
$\Gamma_{0.3-2}$	(0.85, >99.99)	(-0.35, 87.8)	–	–	–	–
$L(0.3-2)$	(0.10, 33.8)	(0.86, >99.99)	(0.12, 39.5)	–	–	–
z	(-0.45, 95.8)	(0.42, 94.0)	(-0.24, 71.0)	(0.39, 91.6)	–	–
$FWHM$	(-0.66, 99.9)	(0.66, 99.9)	(-0.59, 99.5)	(0.39, 91.6)	(0.25, 72.0)	–
R_L	(0.21, 63.2)	(0.29, 79.6)	(0.15, 48.4)	(0.38, 91.2)	(0.03, 10.5)	(0.07, 24.2)
M_V	(0.28, 77.4)	(-0.54, 98.9)	(0.19, 58.5)	(-0.53, 98.7)	(-0.36, 89.0)	(-0.24, 71.0)
M_{BH}	(-0.65, 99.8)	(0.61, 99.7)	(-0.57, 99.4)	(0.30, 81.8)	(0.29, 79.1)	(0.72, 99.98)
\dot{m}	(0.75, >99.99)	(-0.41, 93.4)	(0.71, 99.97)	(-0.05, 17.7)	(-0.09, 29.0)	(-0.76, >99.99)

Appendix A: Notes on individual objects

In this section, we give some notes about each object in our sample. An exhaustive comparison with previous observations for each objects is beyond the scope of the work. For an overview of their X-ray characteristics found with *XMM-Newton*, see Table A.1 where we report for each object the possible presence of a soft excess, of a warm absorber, and of a Fe K line.

All objects of this sample were already observed by *ROSAT* (Wang et al. 1996). The soft photon indices found during the *XMM-Newton* observations (see Table 4) are consistent within the errors for most of the quasars with the *ROSAT* values reported by Wang et al. (1996), except for PG 1114+445, PG 1244+026, and PG 1307+085.

A.1. 1Zw1 ($z = 0.061$)

1Zw1 is the prototype ‘‘Narrow Line Seyfert 1’’ nucleus whose spectrum is widely used as an Fe II template for almost all quasars. This object has already been observed with *ASCA* (Reeves & Turner 2000) and was well fitted with an absorbed power law model (over the 0.5–10 keV energy range) combined with a narrow Gaussian emission line. They found a very soft photon index of $\Gamma = 2.37 \pm 0.05$, and a very large *EW* of 483 ± 212 eV at $6.77^{+0.11}_{-0.17}$ keV. In their data a broad line was only marginally required at a probability of 94.6%. In the present *XMM-Newton* observation, we found that a broad line is statistically required with a probability of 99.8% compared to a narrow line. This line has one of the highest significances of our sample with a probability higher than 99.9%. The energy of the line found here is consistent within the errors with the Reeves & Turner (2000) result. Recently, Gallo et al. (2004) presented a detailed *XMM-Newton* analysis of 1Zw1. As in the present work, they found signatures of a warm absorber. They confirmed the presence of a prominent iron feature, and suggest that the broad emission feature can be attributed to a neutral Fe $K\alpha$ line in addition to a blend of He- and H-like Fe $K\alpha$ lines. The light curve shows a strong, hard X-ray flare mainly in the 3–12 keV band. The timing results are consistent with the flare originating in the accretion disk corona. However the iron emission line(s) did not appear to respond to changes of the continuum flux during the flare.

A.2. PG 0804+761 ($z = 0.100$)

PG 0804+761 was one of the brightest radio-quiet quasars observed by *ASCA* with a energy spectrum well represented by a simple power law model with a photon index of $2.18^{+0.02}_{-0.03}$ in the 2–10 keV energy range with no significant Fe K emission detected (George et al. 2000). Recently, Papadakis et al (2003) found similar results with *RXTE* analyzing the spectrum averaged over one year ($\Gamma_{3-15 \text{ keV}} = 2.10^{+0.12}_{-0.10}$ and no Fe K line is statistically required). The flux variations appeared not to be associated with any spectral variations. During the present *XMM-Newton* observation, we find in the 2–5 keV band a consistent photon index of $\Gamma = 2.19 \pm 0.09$. Combining a narrow Gaussian emission line at 6.4 keV with an absorbed power law

Table A.1. Summary for all objects for detections of soft excess (SE), warm absorber (WA), and Fe $K\alpha$ line.

Source	SE	WA	Fe $K\alpha$ line
Narrow line galaxies (5 objects)			
1Zw1		Yes	Yes (broad at ~ 6.7 keV)
PG 1115+407	Yes		Yes (broad at ~ 7 keV)
PG 1244+026	Yes		Yes (narrow at ~ 6.7 keV)
PG 1402+261	Yes		Yes (blueshifted above 7 keV)
Mrk 478	Yes		
Radio-quiet quasars (14 objects)			
PG 0804+761		Yes	Yes (broad at ~ 6.7 keV)
PG 0947+396	Yes	Yes	Yes (narrow at 6.45 keV)
PG 0953+414	Yes		
PG 1048+342	Yes		Yes (narrow at 6.4 keV)
PG 1114+445		Yes	Yes (narrow at ~ 6.4 keV)
PG 1116+215	Yes	Yes	Yes (broad at ~ 7 keV)
PG 1202+281	Yes	Yes	
PG 1307+085	Yes	Yes	
PG 1322+659	Yes		
PG 1352+183	Yes		
Mrk 1383	Yes		Yes (narrow at ~ 6.6 keV)
PG 1427+480	Yes		
Mrk 876	Yes	Yes	
PG 1626+554	Yes		
Radio-loud quasars (2 objects)			
PG 1309+355	Yes	Yes	Yes (narrow at 6.4 keV)
PG 1512+370	Yes		Yes (narrow at 6.5 keV)

model, we find only weak evidence for such a line (F-test probability of only 92.8%). However, as reported in Table 7, leaving the energy of the line to vary, we find a much better fit for a narrow line at $E = 6.76 \pm 0.06$ keV (F-test probability of 98.5%). Leaving the width of the line to vary gives a probability of 99.7% for the detection of the line. The broad-band continuum is very well fitted by a broken power law model, the combination of a black body and a power law model, and best fitted by a double Comptonization model.

A.3. PG 0947+396 ($z = 0.206$)

PG 0947+396 was observed previously by *BeppoSAX* and its spectrum shown the presence of a line at 6.35 ± 0.13 keV and a large *EW* of 670 ± 170 eV, however the reduced $\chi^2 = 1.44$ was unacceptable ($\Gamma_{1.3-10 \text{ keV}} = 1.95 \pm 0.10$, Table 6 in Mineo et al. 2000). We find for the *XMM-Newton* observation that adding a narrow line marginally improves the fit (F-test probability of 94.9%). The energy of the line at $6.45^{+0.07}_{-0.12}$ keV is compatible with neutral to moderately ionized iron (i.e. Fe XVII). The equivalent width of 92 ± 65 eV is compatible with those observed in RQQ (i.e. a mean *EW* of 163 ± 17 eV, Reeves & Turner

2000). The broad-band continuum is very well fitted either by a broken power law model or by a double Comptonization model. We find no additional significant intrinsic absorption as expected from the weak UV absorption observed in this object (Brandt et al. 2000).

A.4. PG 0953+414 ($z=0.239$)

PG 0953+414 was observed by *ASCA* (George et al. 2000) in November 1997. They found that the spectrum was well fitted by an absorbed power law model with $\Gamma = 2.03^{+0.06}_{-0.05}$. We find that the 2–5 keV spectrum is well fitted by an absorbed power law model with $\Gamma = 2.04 \pm 0.11$, i.e. consistent with the previous observation. Additionally, we found the presence of a soft excess. The broad-band continuum is very well fitted either by a broken power law model, or by a double Comptonization model.

A.5. PG 1048+342 ($z=0.167$)

PG 1048+342 was observed by *BeppoSAX* (Mineo et al. 2000) in May 1997. They found no indication for the presence of a soft excess below 2 keV, and the spectrum was well fitted with an absorbed power law model ($\Gamma = 1.82 \pm 0.07$). We find the presence of a soft excess and that the broad-band continuum is very well fitted either by a broken power law model, or by a double Comptonization model.

A.6. PG 1114+445 ($z=0.144$)

PG 1114+445 was one of the few quasars for which the *ROSAT* PSPC spectrum could not be adequately represented by a single power law model ($\Gamma = 2.36 \pm 0.49$, Wang et al. 1996) and the only quasar (from 23 objects) for which there was strong evidence of absorption by ionized material (Laor et al. 1994). This X-ray absorption feature was also confirmed using *ASCA* by George et al. (1997) who found that the column density of the photoionized medium is about $2 \times 10^{22} \text{ cm}^{-2}$ with an ionization parameter of $U_x \sim 0.1$ (U_x is defined in Eq. (1) in Netzer 1996). Such parameters are similar to those found in Seyfert I galaxies at lower redshift. UV absorption lines of Ly α , C IV, and N V were observed with *HST* by Mathur et al. (1998), who concluded that the mass outflow rate is comparable to the accretion rate in this object.

The *XMM-Newton* observation allows us to obtain a very good S/N spectrum of this object. We confirm the huge absorption in the soft X-rays which is satisfactorily fitted with two absorption edges of O VII (0.74 keV) and O VIII (0.87 keV) with optical depths of about 2.3 and 0.3, respectively. However the determination of the exact nature of this medium (ionization state, velocity, etc.) needs data with higher spectral resolution such as from the RGS aboard *XMM-Newton*. For example, the absorption feature is certainly a complex mixture of absorption lines and edges of Oxygen and Iron as the so-called UTA (Behar et al. 2001). Unfortunately for the present exposure time the S/N of the RGS data is very poor with only about 700 counts (source + background) in each RGS instrument which is too

low for any spectral analysis. Therefore, a longer observation of this object with spectrometers is required to probe the nature of the warm absorbing medium.

A.7. PG 1115+407 ($z=0.154$)

PG 1115+407 is one of the four objects of our sample which displays a narrow optical H β line at 5100 Å with a *FWHM* of 1720 km s^{-1} , and therefore could be associated with a narrow line QSO similarly to NLS1 galaxies. Mineo et al. (2000) found that the *BeppoSAX* spectrum of this object displays a line at $6.69 \pm 0.11 \text{ keV}$ ($EW = 580 \pm 280 \text{ eV}$) similar to those found in NLS1 galaxies and consistent with an origin from ionized gas. The *XMM-Newton* data marginally require the presence of an iron K α line near 7.2 keV. This energy is compatible within the errors with the previous *ASCA* observation, although at this energy the line may be due to higher ionized iron such as Fe XXVI (H-like).

A.8. PG 1116+215 ($z=0.177$)

From an *ASCA* observation, Nandra et al. (1996) found a high significance for a narrow line at $E = 6.90 \pm 0.15 \text{ keV}$ with a large EW of $280^{+160}_{-170} \text{ eV}$. The centroid energy of this line corresponds to very highly ionized iron (Fe XXV–Fe XXVI) and could imply that the accretion disk is ionized as expected from the high ratio UV/X-ray luminosity of this source indicating that it radiates at a substantial fraction of the Eddington limit. Analysing the same *ASCA* data, Reeves & Turner (2000) found also a significant emission line of ionized iron, but at a slightly smaller energy $E = 6.76 \pm 0.08 \text{ keV}$ ($EW = 274^{+155}_{-140} \text{ eV}$). In the present *XMM-Newton* data analysis we found the presence of a very highly ionized line at $E = 6.7\text{--}7.0 \text{ keV}$, corresponding to He-like iron (Fe XXV) to H-like iron (Fe XXVI). A broad or relativistic profile is statistically required and a very large EW is inferred ($EW \sim 500\text{--}900 \text{ eV}$).

A.9. PG 1202+282 ($z=0.177$)

The PG 1202+282 data, in the 0.1–10 keV energy band, were well represented by an absorbed power law model ($\Gamma = 1.97 \pm 0.08$) using *ROSAT* plus *BeppoSAX* data (Mineo et al. 2000). In the present *XMM-Newton* observation we find the clear presence of a soft excess below about 1.5 keV. The broad-band continuum (0.3–12 keV) is very well fitted either by a broken power law model, or by a double Comptonization model.

A.10. PG 1244+026 ($z=0.048$)

PG 1244+026 is one of the five narrow line objects present in our sample, and has the narrowest H β line ($FWHM = 830 \text{ km s}^{-1}$). It has the lowest redshift and an extreme accretion rate relative to the Eddington rate. PG 1244+026 was previously observed with *ROSAT* and *ASCA* which revealed rather steep 0.1–2 keV and 2–10 keV spectra with photon indices of 3.3 ± 0.1 and 2.35 ± 0.12 , respectively (Fiore et al. 1994, 1998). A consistent value of the soft photon

index was reported by Wang et al. (1996) using *ROSAT*. The present *XMM-Newton* observation shows that the data are not well represented by a broken power law. In the soft X-ray range the large soft excess appears more curved than for the other objects. We find that the soft photon index is higher (steeper slope) than that observed with *ROSAT*. The data are well fitted by either a black body plus power law model, or by a double Comptonization model. The temperature inferred for the black body continuum ($kT \sim 197$ eV) is slightly larger than that expected for a standard accretion disk ($kT \sim 73$ eV).

A.11. PG 1307+085 ($z = 0.155$)

From *ROSAT* data, Wang et al. (1996) found a soft photon index of 3.37 ± 0.13 . It was also observed above 2 keV by Lawson & Turner (1997) using *Ginga*. They found that the spectrum was well represented by a simple power law over the 2–18 keV energy range with a photon index of 1.90 ± 0.11 with no detection of a narrow line at 6.4 keV. We find for the pn spectrum below 2 keV a soft photon index of 2.22 ± 0.05 , smaller (flatter slope) than *ROSAT*. The pn spectrum (over the 2–12 keV band) is well fitted by a power law with a photon index of 1.56 ± 0.09 ($\chi^2/\text{d.o.f.} = 114.2/118$, $P(\chi^2) = 58.1\%$). This photon index appears harder than that found previously, however this could be due to real hardening in the 2–12 keV band or to the presence of a reflection component below 12 keV. We do not find any indication of a Fe $K\alpha$ line, which appears to rule out the latter scenario.

A.12. PG 1309+355 ($z = 0.184$)

PG 1309+355 is one of the two radio-loud objects of our sample. It was observed by *ASCA* in 1997, according to the *Tartarus* database¹, the spectrum was well fitted with a simple power law with a photon index of 1.77. This value is compatible with the one we find in the 2–5 keV energy range with *XMM-Newton*. We further detect an iron $K\alpha$ line near 6.4 keV. A broad line is only marginally required with a width of $0.21^{+0.24}_{-0.10}$ keV. If the line is broad, the inferred EW is much higher than the mean value observed for RLQ from *ASCA* data, i.e. 85 ± 15 eV (Reeves & Turner 2000).

A.13. PG 1322+659 ($z = 0.168$)

PG 1322+659 was observed by *ASCA* (George et al. 2000) in May 1999. The broad-band *XMM-Newton* continuum is very well fitted by either a broken power law model, or the combination of a black body and a power law model, or by a double Comptonization model. No significant detection of an iron $K\alpha$ line is required neither at 6.4 keV nor at higher energy.

A.14. PG 1352+183 ($z = 0.152$)

PG 1352+183 was observed previously with *BeppoSAX* by Mineo et al. (2000) who found that the data were well fitted by a single power law model. They also claimed the presence

of a Fe K line at 6.43 ± 0.16 keV, with $EW = 760 \pm 460$ eV, but their detection was at only 1.5σ . With *XMM-Newton*, we find the presence of a significant soft excess below 2 keV with a soft X-ray photon index $\Gamma = 2.69^{+0.10}_{-0.08}$. We find no Fe K line, however near 6 keV the S/N is not high enough to detect a weak line.

A.15. PG 1402+261 ($z = 0.164$)

PG 1402+261 is a narrow-line quasar observed previously with *BeppoSAX* by Mineo et al (2000). They found that the data were satisfactorily represented by a broken power law continuum with $\Gamma = 2.59 \pm 0.10$ and 1.52 ± 0.30 for the soft and hard X-ray band, respectively. They did not report any detection of a Fe K line, however the MECS spectrum shows a large positive deviation above 7 keV in the observer frame, compared to a power law continuum fit. PG 1402+261 is one of the most interesting objects of the present *XMM-Newton* sample. It shows a very large positive deviation from 5 keV to 9 keV (in observer frame). This could be interpreted as a very large Fe K line highly blueshifted, however other explanations, such as partial covering, are not ruled out (Reeves et al. 2004).

A.16. Mrk 1383 (PG 1426+015, $z = 0.086$)

Mrk 1383 was previously observed above 2 keV with *Ginga* in January 1991 (Lawson & Turner 1997). The spectral fitting gave a photon index of 2.07 ± 0.20 . We find here a 2–5 keV photon index of 1.95 ± 0.13 which is consistent with that found by *Ginga*.

A.17. PG 1427+480 ($z = 0.221$)

PG 1427+480 was observed by *ROSAT* and the spectrum was well represented with a power law with $\Gamma = 2.37 \pm 0.27$. No observation above 2 keV has been reported until now. Therefore the present *XMM-Newton* observation allows to study the hard X-ray emission for the first time. The source shows a soft X-ray excess and the soft X-ray photon index ($\Gamma = 2.52^{+0.08}_{-0.03}$) is higher than the hard photon index ($\Gamma = 1.90 \pm 0.12$). We find neither the presence of a warm absorber nor the presence of a significant Fe K line.

A.18. Mrk 478 ($z = 0.077$)

Mrk 478 (PG 1440+356) is one of the five narrow line objects of our sample. From *ROSAT* observations, Wang et al. (1996) inferred a soft photon index of 3.43 ± 0.23 . It has been observed with *ASCA* (Vaughan et al. 1999) and a good fit was found using a combined black body/power law model with $kT_{\text{bb}} = 89 \pm 0.12$ and $\Gamma = 1.96 \pm 0.05$. Reeves & Turner (2000) detected a soft excess and found a Fe $K\alpha$ line at 6.37 ± 0.07 keV with $EW = 191 \pm 119$ eV (detection at 97%). Mrk 478 was observed recently (August 8–9, 2000) using the *Chandra* Low Energy Transmission Grating spectrometer, and no significant emission or absorption feature were detected (Marshall et al. 2003). Combining with *BeppoSAX* data,

¹ <http://tartarus.gsfc.nasa.gov/>

they found that the spectrum is well fitted with two power laws with $\Gamma_{\text{soft}} = 3.03 \pm 0.03$ and $\Gamma_{\text{hard}} = 1.4 \pm 0.2$. They suggested that the X-ray continuum may result from Comptonization of disk thermal emission in a hot corona through a range of optical depths. In the present *XMM-Newton* data, we also find that the spectrum is well fitted by the combination of a black body with a power law model, but it is much better fitted either by a broken power law model, or a double Comptonization model. Here we found $\Gamma_{\text{soft}} = 3.12^{+0.07}_{-0.06}$ and $\Gamma_{\text{hard}} = 2.45 \pm 0.13$. The present soft spectrum has a similar shape as the one found with *ROSAT* ($\Gamma = 3.43 \pm 0.23$), while the hard spectrum appears to be slightly softer compared to the *BeppoSAX/MECS* observation ($\Gamma = 2.19 \pm 0.05$, Marshall et al. 2003).

A.19. PG 1512+370 ($z = 0.371$)

PG 1512+370 is one of the two radio-loud objects of our sample and has the highest redshift. The *XMM-Newton* broad-band continuum is very well fitted either by a broken power law model, or by a double Comptonization model. An iron $K\alpha$ line is detected with a F-test probability of 94.4%. The energy of the line is 6.51 ± 0.13 keV which is compatible with neutral to moderately ionized iron.

A.20. Mrk 876 (PG 1613+658, $z = 0.129$)

Mrk 876 was previously observed above 2 keV with *Ginga* by Lawson & Turner (1997). They found a photon index in the 2–18 keV of 1.63 ± 0.03 which is rather flat for a RQQ quasar. No Fe K line was reported. In the present *XMM-Newton* observation, we are able to constrain both the soft and hard X-ray slopes in this object. Mrk 876 shows the presence of a soft excess and a warm absorber below 1 keV, and no evidence for a Fe K line.

A.21. PG 1626+554 ($z = 0.132$)

PG 1626+554 was observed by *BeppoSAX* in February 1998 by Mineo et al. (2000). They found an unusual large excess below 0.2 keV. They inferred that such an “ultra-soft” excess could be the tail of a very steep unusually strong thermal component. Moreover, this “ultra-soft” excess could be related to the unusually flat optical to soft X-ray slope $\alpha_{\text{ox}} = -1.139$ (Laor et al. 1997). In the present *XMM-Newton* observation, we found that this object does not show a soft excess between 0.3–2 keV, but due to the present energy band we are not able to confirm the “ultra-soft” excess found previously below 0.2 keV.